SANDIA REPORT SAND82-1701 • Unlimited Release • UC-63
Printed September 1982

SAND--82-1701
DE83 000803

Fundamental Studies of Grain Boundary Passivation in Polycrystalline Silicon With Application to Improved Photovoltaic Devices

A Research Report Covering Work Completed From February 1981 to January 1982

Carleton H. Seager, David S. Ginley

Prepared by
Sandia National Laboratories
Albuquerque, New Mexico 87185 and Livermore, California 94550
for the United States Department of Energy
under Contract DE-AC04-76DP00789

DISCLAIMER

Issued by Sandia National Laboratories, operated for the United States Department of Energy by Sandia Corporation.

Printed in the United States of America
Available from
National Technical Information Service
U.S. Department of Commerce
5285 Port Royal Road
Springfield, VA 22161

NTIS price codes
Printed copy: A04
Microfiche copy: A01

Unlimited Release

FUNDAMENTAL STUDIES OF GRAIN BOUNDARY PASSIVATION IN POLYCRYSTALLINE SILICON WITH APPLICATION TO IMPROVED PHOTOVOLTAIC DEVICES

A Research Report Covering Work
Completed from February 1981 to January 1982
under SERI Subcontract No. DS-0-9109-1 by

C. H. Seager and D. S. Ginley
Sandia National Laboratories
Albuquerque, New Mexico 87185

THIS PAGE

WAS INTENTIONALLY

LEFT BLANK

C. Future Kaufman Source Studies.....24

D. Solar Cell Passivation Using the d.c. Discharge....25

Table I - Honeywell Silicon-on-Graphite AM1 Parameters.....26

Table II - Solar Cell Improvement Using d.c. Discharge Passivation Honeywell Silicon-on-Ceramic Large Grained Material.....27

References.....28

Figure Captions.....29

Appendices.....34

PREFACE

This report is an account of the work performed under U.S. Department of Energy Contract No. DE-AC04-76-DP00789 from February 1, 1981, to January 1, 1982. Principal investigators are C. H. Seager and D. S. Ginley; the program manager is G. A. Samara.

Abstract

Grain boundary barrier heights and other properties were measured on a variety of Wacker poly-Si to test the contention of Redfield that as received samples had no potential barriers and that temperature anneals activate the impurities in the boundaries. Our results show that these generalizations are not true and that a variety of barrier behaviors are found. Several of our new analytical techniques for studying grain boundaries and their passivation have been upgraded, including a new cell for FTIR studies, electrochemical techniques, and a laser scanning apparatus for imaging grain boundaries. Grain boundaries in a variety of samples have been successfully passivated by the use of both the Kaufman ion source and a d.c. discharge apparatus. 20% improvements in cell efficiencies have been observed in large grained poly-Si cells, and the time of treatment has been drastically reduced.

Table of Contents

Preface....iv

Abstract....v

I. Introduction....1

II. Fundamental Grain Boundary Studies....4

A. Studies of Grain Boundary Barrier Heights in N and P Type Wacker Polycrystalline Silicon....4

I. P-type Wacker Silso (2 Ω•cm)....6

a. As received....6

b. After high temperature anneals....7

II. n-type Wacker Silso (3 Ω•cm)....7

a. As received....7

b. After thermal anneals....8

B. Fourier Transform Infrared Specroscopy of Grain Boundary Bonded Hydrogen....9

C. Electrochemical Measurements of Virgin and Passivated Grain Boundaries....15

III. Studies of Grain Boundary Passivation....17

A. Kaufman Ion Source Passivation and Modeling....17

B. Future Kaufman Source Studies....18

C. d.c. Discharge Passivation Studies....19

D. Future Plans....21

IV. Solar Cell Passivation Studies....22

A. Treatment of RCA Epitaxial Solar Cells....22

B. Preparation and Characterization of Honeywell Silicon-on-Graphite Solar Cells....22

INTENTIONALLY LEFT BLANK

I. Introduction

Polycrystalline silicon solar cells offer the potential for inexpensive, maintenance free electrical power production. For that potential to be realized processes must be developed to minimize the undesirable effects of the grain boundaries in these devices. We and others have shown that the introduction of atomic hydrogen into polysilicon devices is one promising method of passivating grain boundaries. The present report details our research progress over the period January-December 1981 in a DOE/SERI funded program designed to understand and optimize this passivation technique.

As in past reports we have divided our discussion of this progress into three separate categories. In the first (Sec. II) we detail our efforts to model the band structure and electrical transport properties of single silicon grain boundaries. In this research period we have examined the contention of Redfield that heating grain boundary structures above 600°C causes them to be electrically active, (i.e., possess substantial barrier heights) and that this activity is caused by oxygen segregating to the boundaries. Grain boundaries in both n and p-type Wacker Silso polysilicon were examined in the as-received state and after various thermal annealing schedules. Some effects of heat treatment were seen, but the uniformity of behavior implied by Redfield was not observed. We have used these data and other experiments to draw some conclusions about the relative importance of intrinsic versus extrinsic grain boundary trapping states.

We have also begun work on characterizing silicon-electrolyte interfaces as a possible means for rapid evaluation of the passivation process. Also included in this section are the details of our Fourier transform infrared spectroscopy studies. Construction of a sophisticated, in situ sample cell for high temperature studies of the infrared active SiH bonding modes has been completed. The features and complexities of this cell are discussed in some detail.

In Section III of this document we present a summary of our attempts to optimize two separate grain boundary hydrogenation procedures. Detailed variation of the operational parameters of the Kaufman ion source have been completed and a simple model describing the experimentally observed variations of the effectiveness of this process has been formulated. We also discuss the results of varying the operational characteristics of the simple parallel plate d.c. discharge. Despite the simplified nature of the apparatus involved in this technique, results comparable to the ion engine technique are achievable. Larger versions of this apparatus will be built in the near future.

In Section IV the results of preparing and passivating several types of polycrystalline silicon solar cell devices are presented. While the improvements in large grain devices are impressive and represent large time savings over previously reported passivation attempts on these devices using a low pressure glow discharge plasma at RCA, the true objective of our program

continues to be the characterization and passivation of small-grained silicon solar cells. We detail the preparation and characterization of some recently completed polysilicon solar cells having grain sizes of the order of 100 μm. Treatment of these devices is scheduled for the next research period.

Finally, Appendices A, B, and D are copies of published papers generated during this research period. In many cases the detailed nature of our investigations is contained in these papers in order to accommodate those readers who wish to delve deeper into the subject matter. Appendix C presents the design of our FTIR high temperature sample cell.

II. Fundamental Grain Boundary Studies

A. Studies of Grain Boundary Barrier Heights in n and p type Wacker Polycrystalline Silicon

In a recent publication[1] Redfield has commented that as-received Wacker Silso polycrystalline silicon has very few or no grain boundary potential barriers, but that short anneals at 600 - 900°C in an inert atmosphere "activate" the grain boundaries. This effect was reported on both n and p-type Wacker poly[1,2]. Redfield uses these data to argue that as-received grain boundaries are in general not electrically active, and that activation is caused by oxygen segregation occurring during the annealing cycles. Although his paper[1] is a bit vague on this point - the implication is that all grain boundaries - not just those in Wacker Silso - depend on impurity effects for their electrical activity.

We find the implications of this proposal disturbing for several reasons:

1. We have examined a variety of types of polycrystalline silicon including:

   a. TI 25 μm grain CVD poly, NTD doped.

   b. Monsanto float zone poly, NTD doped.

   c. Monsanto float zone poly, melt doped.

   d. Sandia deposited in situ doped CVD poly, n and p type.

   e. Honeywell silicon-on-ceramic poly, boron doped.

   f. Honeywell silicon-on-graphite poly, boron doped.

In all these cases substantial grain boundary barrier heights are seen without deliberate, after preparation anneals. Furthermore the maximum barrier heights (in the weakly doped materials) are remarkably similar. It would surprise us if a similar degree of oxygen segregation was present in all these materials.

2. Recent investigations by Johnson[3] have identified the ESR signal in CVD poly with grain boundary states. The g value for this signal is essentially identical to that for the dangling bond resonance seen in amorphous silicon[4]. Since dangling bond states are known to be associated with dislocations and many grain boundaries have been shown to contain arrays of dislocations (which are known to be electrically active[5], themselves), it would appear surprising if the intrinsically present grain boundary states did not play some role in the electrical activity of grain boundaries.

3. Wacker Silso material is cooled very slowly from the casting temperature and it would seem somewhat unlikely that all the impurity segregation needed to explain this grain boundary-effect should occur during the rather brief reheating process that Redfield has employed. For these reasons, attributing most of this activity to extrinsic states does not at present appear to be a well-founded assumption.

In order to establish a data base for further discussions of this subject, we have obtained both n and p-type Wacker Silso wafers and have carried out experiments on the effect of heating on the grain boundary potential barriers in this material. Bars

of dimension ~ 1 x .1 x .03 cm were cut from these wafers and ohmic contacts were applied on each end to inject current from a constant current supply. The voltage drop across grain boundaries normal to the long axis of the bars were measured with a surface potential probe (in the absence of light). By choosing the outermost portions of these wafers it was possible to have the grain size large enough that most of the boundaries bisected the samples, causing the current to flow across each boundary plane in succession. In some cases the temperature dependence of these boundary impedances were measured from 5 to 90°C. Thermal anneals were carried out in Argon, N_2 or vacuum at temperatures from 400°C to 900°C. In many cases surface oxide removal via HF etching or substantial material removal using the Sirtl etch was employed to ascertain whether the observed impedances were dominated by surface shunting effects. Because of the great number of boundaries studied and the variety of effects observed, a generalized summary of the results is given below (with a few detailed examples) rather than a detailed enumeration of the behavior of each boundary. We will break the discussion down by doping type.

I. p-type Wacker Silso (2 Ω·cm)

a. <u>As Received</u> - A variety of barrier impedances (and activation energies) are seen. Some of these barrier impedances are the largest we have ever observed in p-type silicon. Honeywell SOC polysilicon, for example, has barriers which are 10-50 times less resistive. An example of the temperature dependence of one of these large barriers is seen in Figure 1. If the activation

energy seen here is truly representative of a saturated or largest barrier, then this energy should be $\approx E_{FB} - E_V$, where E_{FB} is the neutral level of the trap state energy distribution at the grain boundary and E_V is the energy of the valence band edge. In fact the neutral level inferred from this activation energy, 0.47 eV above the valence band, is close to that which we have deduced for barriers in n-type silicon[6]. The major point to be made here is that unannealed p-type Wacker Silso has an abundance of "active" grain boundaries.

b. After High Temperature Anneals - 40 minute anneals performed in N_2 or Ar at 700°C or 900°C almost always reduced grain boundary impedances. This was not just a surface effect but permeated to the center of the boundary plane. These changes were typically factors of 2 to 5 in impedance. As we have seen before, atomic hydrogen exposure performed below 400°C after these anneals essentially eliminated all electrical evidence of the boundaries.

II. n-type Wacker Silso (3 Ω·cm)

a. As Received - As in the p-type case a variety of barrier impedances are seen in the unannealed samples. However, it is observed that none of the impedances are as large as those we have measured in other n-type polysilicon. The largest barriers are roughly 1-2 decades less resistive than those reported on in our studies of NTD doped TI[7] and Monsanto float-zone polycrystalline silicon[6], for comparable doping levels. This implies barrier

heights 100 to 150 mV less than those previously reported in n-type polycrystalline silicon.

b. After Thermal Anneals - Several of our samples were successively annealed in N_2 for one hour from 400°C to 700°C in 50°C steps. A variety of behaviors was evident. A few (10-15%) of the barriers, increased markedly (as much as 2 decades). The rest changed only mildly (factors of 2-3) or not at all. Many of the barriers which increased had the majority of their change occur by 500°C where oxygen diffusion is expected to be exceedingly slow. Some actually decreased with thermal annealing, as was commonly seen in the p-type case. The barriers that tended to increase drastically were clustered in particular sections of the Silso wafer.

Discussion

Several overall comments can be made about our data. The first is that unannealed Wacker has electrically active barriers. In the p-type material they are fairly large in some cases, but for n-type Silso they are quite a bit smaller than one would expect from experience with other types of polysilicon. Thermal annealing produces a mixed bag of results. Some barriers in n-type Silso increase markedly while others decrease or do not change. The barriers in p-type Silso practically always decrease with heat treatment in Ar or N_2. One possible explanation for the sensitivity of some barriers in Wacker is that the Wacker casting process produces large residual strains which can relax

more easily after a thin sample is cut from the boule. The residual strains or their relaxation could affect the structure of the boundary, increasing some barrier heights while decreasing others. This could explain why reheating sliced samples causes changes which did not already take place during the original slow cool from casting. A simple test of this would be to subject a large boule of Wacker to 700 → 900°C anneals for extended periods before sample slicing. If subsequent short anneals in this temperature range produced marked barrier height changes in samples cut from this boule, stress effects would appear to be the culprit. This is particularly so since little effect of the annealing atmosphere on these changes has been noted.

At this stage of our experimentation we must admit to seeing no universality of heat treatment behavior as Redfield has implied, and certainly no reason to favor oxygen effects as the explanation for the changes that are seen. It is possible that some of the differences between his and our data could arise from our preference for measuring the bigger grains located near the edge of the wafer. Wafer to wafer variations can also not be ruled out as another source of these differences.

B. Fourier Transform Infrared Spectroscopy of Grain Boundary Bonded Hydrogen

The ability to do in situ annealing or passivation of polysilicon samples while monitoring the infrared spectra should greatly increase our understanding of the kinetics of diffusion and of hydrogen into and out of the polysilicon. We have already demonstrated that Fourier transform infrared spectroscopy is a useful

tool to monitor grain boundary and surface hydrogen (Appendix B). We have observed recently however that there are quite a few sites associated with the boundaries and that redistribution between these sites is a function of both temperature and time. For example, IR spectra obtained from partially annealed samples show an initial migration from SiH_2 sites to SiH centers located in the grain boundaries. Also, a series of IR spectra vs position have been obtained with fine grained Monsanto polycrystalline silicon that was lightly neutron transmutation doped so that grain boundary impedance measurements could be performed. These experiments indicate qualitatively that increases and decreases in grain boundary impedance are followed by decreases and increases in the intensity of the 2019 cm^{-1} peak as a function of both position and treatment. The 2019 cm^{-1} absorption has been associated with SiH located at the grain boundaries.

The fact that complex site migrations and positional dependences of the FTIR spectra for grain boundary hydrogen were observed in a large number of polysilicon samples led us to spend a predominate part of this last period designing and constructing an infrared cell with capabilities for in situ annealing and passivation experiments. Appendix C contains a copy of the plans for the cell which is quite unusual and complex. An internally heated inconel (or stainless steel) sample holder will be placed within a water cooled quartz cell with KBr infrared transmitting windows. Water cooling of the windows is required to protect

them from thermal shock and to potentially allow sample temperatures up to the design limit of 800°C to be achieved. The cell is designed to hold two silicon samples either a) maintained in a high vacuum (10^{-6} torr or better) or b) in a flowing gas environment. Temperature is measured and controlled by a type K thermocouple held in contact with one of the silicon samples. The inconel sample holder is heated with an inconel sheathed nichrome wire heater with a maximum temperature capability of 1000°C. The heating element is brazed into a machined groove in the sample holder to ensure intimate thermal contact. Although the sample holder has been designed with minimum surface area and maximum heating element windings, the 38 cm length of the heating element is not sufficient to attain the 800°C design limit. The major heat loss mechanism at the design temperature is by radiation. Oxidized inconel has a measured emittance of 0.55 at 100°C. (The emittance ε at 800°C is expected to be slightly greater but instruments capable of this measurement are not available at Sandia). The calculated heat losses for the 40 cm^2 inconel sample holder at 800°C are therefore expected to be 166 watts while the maximum thermal input from the heater is only 130 watts. Conduction and radiative losses from the samples will increase this disparity. The spectrometer sample compartment unfortunately limits the size of the IR cell to near that shown and therefore eliminates the use of radiation shields. Temperatures below 800°C would provide some useful data but the full temperature range is required

for definitive experiments. Consequently a low emittance coating must be used to achieve the desired 800°C sample temperatures.

Initially, sputtered Rh was selected due to its extremely low emittance ($\varepsilon_{100} \approx 0.04$), high temperature stability and inert behavior in the environments to be studied. However, studies of Rh sputtered on inconel revealed that the low ductility and thermal expansion mismatch were such that the Rh layer cracked and allowed the inconel elements to thermally diffuse above the Rh layer after one hour at 800°C. Therefore the ε_{100} increased from 0.04 to 0.55. Platinum was selected as a next best alternative. Pt has twice the emittance of Rh, does not oxidize, and is considerably more ductile than Rh. Unfortunately, the effects of Pt sputtered on inconel were also lost after an hour at 800°C due to diffusion of the Pt below the surface of the inconel ($\varepsilon_{100} = 0.068$ before heating and $\varepsilon_{100} = 0.58$ after one hour at 800°C in air). A diffusion barrier was consequently required. This was achieved by first sputtering Cr followed by air oxidation at 800°C followed by sputtering 1 μm of Pt. The thick chromium oxide layer exhibits excellent diffusion barrier capabilities, with the following measured emittances: as received $\varepsilon_{100} = 0.068$, 7 days at 800°C in air, $\varepsilon_{100} = 0.077$, 21 days at 800°C $\varepsilon_{100} = 0.086$. The emissivity after 21 days at 800°C results in a radiant heat loss of 26 watts at 800°C which is substantially below the 130 watt capabilities of the heating element. Long term 800°C operation should be possible with the current cell design.

Although inconel is our material of choice for the sample holder, extreme difficulties have been encountered in the numerous brazing operations required for this sample holder design (probably due to the formation of molybdenum oxides). Therefore future sample holders will be made from 304 stainless steel. This material is easier to machine and much easier to braze. Similar emittance tests have been performed on 304 ss with Pt sputtered over Cr_2O_3 barrier layers. The initial emittance is $\varepsilon_{100} = 0.069$. Without the Cr_2O_3 layer the Pt is lost on the 304 ss and the emittance reaches 0.655 after one hour at 800°C in the air. After eight days at 800°C in air with the Pt over a barrier layer the emittance is $\varepsilon_{100} = 0.078$. Again this is an effective low emissivity coating for the stainless steel. To avoid materials capability problems with the silicon samples, they will be held in 304 ss or Ta inserts in the sample holder.

In addition to the construction of the IR cells work has progressed on the mounting of the infrared cells on computer controlled positioners supported outside the spectrometer benches. Thus the IR cells will move through a bellows seal into the spectrometer sample compartment. The high quality N_2 purge will therefore be maintained and automatic and accurate ($\pm$ 2 μm) positioning of each sample in the IR beam will be achieved.

Future Directions

We recently received and completed preliminary testing on the Inconel IR sample chamber. Initial testing showed that temperatures of 700°C were easily attainable and we have confidence that the design limit of 800°C is attainable.

The first set of experiments for the cell will be the controlled annealing of passivated bulk fine grained Dow corning and Monsanto polycrystalline silicon. The initial samples will be undoped but NTD samples will be employed as well so that parallel electrical measurements can be made. Both the AC and DC plasma systems will be employed. The object of these studies is to confirm the previous data on the stability of the passivation process by identifying the temperature at which hydrogen loss occurs. A detailed mapping of the rearrangement energies for the various sites will be obtained by a controlled series of controlled temperature soaks. These will be done both by ramping temperature and by monitoring the Si-H stretch modes at a constant temperature. These studies will also try to identify the mechanism of hydrogen diffusion from the surface by monitoring changes in the known "surface" peaks.

Over the long term two other types of experiments employing this cell are envisaged. The introduction of a positive electrode will enable a plasma to be struck between it and the sample holder if an appropriate pressure of hydrogen is present. This should for the first time allow for an examination of the hydrogen in-diffusion process. Importantly the intermediate surface states should be identifiable and we should be able to distinguish if they are different than those observed during the outgassing experiments.

C. Electrochemical Measurements of Virgin and Passivated Grain Boundaries

One of the difficulties in optimizing the plasma processes, is that the fabrication of a device structure is normally required to obtain data on recombination center densities. It has been observed in photoelectrochemical (PEC) experiments that excellent Schottky barriers are frequently obtained simply upon contact of a semiconductor with an electrolyte. This interface may be examined by the standard I-V and C-V techniques to obtain considerable information about the semiconductor. This structure is also photoactive giving rise to the energy conversion aspects of these devices. It is our feeling that combining Si with an appropriate electrolyte and then employing LBIC may provide rapid evaluation of the passivation process.

Previously we have done some experiments which indicate, that while inefficient, electrochemical passivation does work. p-type Monsanto samples cathodically biased in 0.01 and 0.1 molar HF electrolytes showed reductions in grain boundary barrier heights. We intend to couple LBIC measurements with in situ passivation attempts in a PEC device. In addition we are going to add the capability of digital image processing to the laser scanning system. This has a number of advantages over any currently existing systems in that data can be attained more rapidly, processed automatically in digital form and computer based image enhancement techniques can be employed. Using the existing models this should allow us to directly obtain the important grain boundary minority carrier parameters.

The photoelectrochemical system will also be employed to investigate a range of passivating agents including hydrogen as a function of voltage, current, illumination, and electrolyte composition. Treatment effectiveness can be continuously monitored by doing in situ laser scans.

III. Studies of Grain Boundary Passivation

A. Kaufman Ion Source Passivation and Modeling

In this research period we have also been concerned with modeling and optimizing the hydrogen passivation process for grain boundaries using a clean, characterizable, hydrogen source. As discussed in previous reports[8], the Kaufman ion engine is a reasonable choice for this source since ion energy, flux, and sample temperature can all be varied independently. We have varied these parameters, one at a time, and explored their effect on grain boundary recombination using EBIC traces to optimize sample treatment conditions. A full description of these experiments as well as a simple diffusion model which explains the overall trends in this data is given in the reprint reproduced in Appendix A.

In brief, these experiments have shown that at 200°C to 350°C, hydrogen diffusion, probably occurring largely down grain boundaries[3], is rapid enough to deplete the sample surface of hydrogen unless sufficiently high ion fluxes are employed. Ion energies above 1 keV are also beneficial, apparently because deeper implantation raises the probability that a hydrogen atom will diffuse into the polysilicon rather than back to the surface where H_2 formation and evaporation can occur. By combining high dose rates and high ion energies we have speeded up the hydrogenation process factors of 10 to 100 over our best audio frequency glow discharge plasma results.

B. Future Kaufman Source Studies

It is apparent from a perusal of Appendix A that there is a great deal of difference in the degree to which each boundary passivates in a given sample of Honeywell polysilicon. This in turn implies that the average improvement number that we have defined for each sample varies from run to run, even under nominally identical treatment conditions. Because the scatter in our EBIC improvement ratio is large enough to make further optimization of the process difficult (using a more detailed matrix of parameter variations), we will address the issue of this scatter. Samples will be treated, outgassed at 600°C to drive off the grain boundary hydrogen, and finally retreated at a different location in the ion beam to establish whether variations in treatment effectiveness are characteristic of certain barrier properties or are caused by differences in local ion fluxes or possible gradients in sample temperature. We will also attempt to passivate Schottky devices to ascertain whether differences in the emitter layers (more or less impurity segregation at certain boundaries, for instance) could cause the observed variations in treatment effectiveness.

We will also explore the issue of whether taking an average of the changes in a large number of barriers might be appropriate in optimizing the hydrogenation procedure. Measurements of the red and infrared quantum efficiency of a fine grained p/n device (such as those fabricated using laser annealing[10] by R. T. Young at ORNL) might be a convenient method for accomplishing this average without unduly lengthy measurements. The overall aim of

the program in this area will of course remain one of speedy, optimum, device improvement using an atomic hydrogen source.

C. d.c. Discharge Passivation Studies

In addition to the Kaufman source, work is continuing on the optimization of the d.c. plasma system. While the ion source is not as clean and monoenergetic the results are comparable and the apparatus is appreciably simpler. Unfortunately there appears to be only a partial crossover between the optimum parameters for the Kaufman source and those for the d.c. source.

The optimum temperatures for the d.c. source are somewhat higher than those for the Kaufman source, being in the range from 290°C - 450°C. Part of the explanation for this may be in the fact that, although we have high plasma densities in the d.c. discharge (system pressures range from 1 - 10 torr), ion energies are low with accelerating potentials ranging from 400 - 600 V. The higher temperatures may be necessary to overcome the smaller ion penetration distances.

We initially noted some visible inhomogeneities in the plasma. Though these did not show up in the EBIC of smaller passivated samples, an effort was made to obtain a uniform plasma that would be required for larger samples. We found that the key requirements are that the top plate is larger than the bottom plate and that the bottom plate is circumferentially surrounded by an insulator. This was accomplished by inserting it into a boron nitride base. All leads were introduced through alumina tubes that fit intimately into the BN form. Temperature was measured and controlled by

spot welding a type K thermocouple directly to the underside of the base plate. It was found that electrical contact between the sample and the base plate (negative potential) was required for optimum results, though considerable passivation occurred without. contact. This was accomplished by spot welding small clips to the base plate to hold the samples down. Initially all of the electrodes and clips were fabricated from tantalum to ensure that they were chemically inert with respect to the silicon, recently however 304 stainless steel has been employed with good results. Figure 2 shows before and after EBIC traces for a Honeywell silicon-on-ceramic sample passivated in the stainless d.c. system. Preliminary tests have also been made on the scale up potential of the d.c. concept. There at present seems to be no problem in constructing a two plate apparatus large enough to treat any of the current polysilicon cells. Based on known d.c. sputtering systems, square meter sized systems are realistic.

In addition to continuing to optimize the d.c. system, we have continued to investigate other potentially interesting plasma reagents. The work on F_2 and O_2 is enumerated in Appendix D. The basic conclusions from this study were that in molecular or atomic form these two reagents increased grain boundary potential barriers in n-type polysilicon. Little effect was observed on p-type material. Current work is concentrating on evaluating the effects of nitrogen (from N_2) and carbon (from CH_4 and C_2H_2) upon the grain boundaries and surface of polysilicon samples. To date

nitrogen effects seem to be similar to oxygen in that grain boundary impedances increase at least for n-type material upon exposure to N_2 plasmas. Little effect is observed with molecular N_2. Silicon surfaces show definite signs of nitriding as well. Figure 3 illustrates some preliminary IR data for a single crystal sample exposed to a 1.3 torr N_2 plasma at 600°C. The carbon results have been very ambiguous so far, the primary observation being the deposition of something resembling polyacetylene on the sample surface.

D. Future Plans

A continued optimization of the d.c. plasma apparatus is planned. Current results seem to indicate that a two minute high temperature (plasma) soak (450°C) followed by a two minute low temperature soak (290°C) results in the best solar cell improvements. In conjunction with the IR experiments we hope to be able to focus on which hydrogenated states are the most important to produce and to optimize treatment parameters to obtain them. A more complete examination of materials compatibility will be made to determine which types of materials might be employed in practical systems. When the above named parameters are determined we plan on constructing a large area prototype system with a treatment area of approximately 125 cm^2.

We will continue our investigation of alternative gaseous reagents. Attention will be directed to electropositive elements which might be effective passivation agents.

IV. Solar Cell Passivation Studies

A. Treatment of RCA Epitaxial Solar Cells

In this past research period we procured several polycrystalline silicon solar cells fabricated with an epitaxial layer of silicon on refined metallurgical grade Si substrates. Full details of cell fabrication, treatment, and characterization are contained in the reprint reproduced as Appendix A. Despite the relatively large grain size of these cells (in the mm range) 10-20% improvements in cell efficiencies were seen after passivation, largely as a result of increases in cell fill factors. We also documented a noticeable ($\sim$ 15%) decrease in surface reflectivity after Kaufman ion source treatment indicating the presence of a thin (100 - 400 Å) surface layer of SiH_x material. This produced some enhancement of J_{sc} in these non-AR coated devices. It should be noted that only a few minutes of treatment with the Kaufman source produced larger efficiency gains than those reported by Robinson and D'Aiello[9] after a two hour exposure to a lower pressure, RF discharge hydrogen plasma.

B. Preparation and Characterization of Honeywell Silicon-On-Graphite Solar Cells

As was mentioned in our last report[8] graphite dip coated with silicon appears to be a reasonable candidate for the fabrication of solar cells useful for demonstrating the effects of hydrogen grain boundary passivation. This material, utilizing high purity POCO graphite, was produced in considerable quantities early in

the Honeywell dip coating process development. We have been provided some of this SOG (silicon-on-graphite) silicon by J. D. Zook of the Honeywell Corporation. Because of its small grain size (typically 100 μm between parallel, columnar grains) and high purity substrate it is hoped that the primary limitations on cell efficiency will be due to grain boundary effects.

We have prepared some prototype cells for passivation using phosphorous ion implantation (2×10^{15} cm^{-2} dose at 120 keV) and thermal annealing. Front gridwork was photolithographically defined with a W/Ag metallization pattern. After the thermal anneal to remove the implantation damage the back cell contact (Si/Graphite) was found to have an unacceptably high resistance - whether this occurred because of the high temperature soak is not known. In any case it was necessary to fabricate a front "back contact" using a sintered Ti/Pt/Au guard ring surrounding the mesa etched central portion of the cell. Because of the small area of the device (typically ~ 0.20 cm^2) and reasonable base doping density (5×10^{16} cm^{-3} boron), this gave us a base contact geometry capable of carrying Air Mass 1 currents without excessive lateral voltage drops across the base of the cell. The fact that the grain boundaries are mostly parallel undoubtedly helped to keep these drops down to a reasonable level (< 5 mV)

The AM1 parameters of the first group of these cells to be fabricated are listed in Table 1. The efficiencies of these non-AR coated devices are fairly low, due to a combination of poor current collection and leaky p/n junction properties. The average values

of J_{sc} are well below the typical values for this parameter for the best Honeywell silicon-on-ceramic cells after accounting for reflection losses. We speculate that this is largely due to the considerably smaller grain size characteristic of this material. Treatment of these recently completed devices is scheduled for our next reporting period.

C. Future Kaufman Source Studies

In addition to passivation of the Honeywell SOG cells mentioned above we are hoping to collaborate with other investigators making polycrystalline silicon solar cells. One possibility for collaboration is the program of R. T. Young at ORNL. Dr. Young has recently reported[10] over 2% efficiencies on cells fabricated from 10 μm grain size Monsanto CVD polysilicon. The junctions in these devices are ion implanted and laser annealed, a procedure which appears to result in much better AM1 efficiencies than the traditional thermal damage anneals. The small grain size of these devices would appear to put them in a regime where grain boundary effects must dominate solar cell properties.

D. Solar Cell Passivation Using the d.c. Discharge

Most of our solar cell work in this reporting period has employed Honeywell silicon on ceramic n-on-p solar cell material as a probe for process optimization. A material with a junction is useful to expedite EBIC and LBIC studies. Some of our results are summarized in Table II. Here we illustrate our best treatments and average treatments in terms of EBIC and Air Mass One efficiency results. In general our results parallel those from the Kaufman source. Figure 4 shows the before and after passivation I-V traces for a Honeywell cell and a two minute d.c. plasma treatment. All of the efficiency results are reported without anti-reflection coatings.

Future Work

In the next research period we intend to concentrate on other types of solar cell materials. These will be the Honeywell silicon on graphite and ORNL fine grained thin film materials. Efforts will be made to treat large area devices. A program will be instituted to develop an in house diffusion system for junction formation. This will hopefully enable us to take virgin films and use an appropriate n-or-p diffusant for junction formation. We can then apply contacts compatible with the passivation process. Work is currently in progress to achieve these ends.

TABLE I

HONEYWELL SILICON-ON-GRAPHITE* AM1** PARAMETERS***

CELL DESIGNATION	CELL AREA (cm^2)	J_{sc} (mA cm^2)	V_{oc} (Volts)	FILL FACTOR	EFFICIENCY %
HSOG-C	0.193	17.2	0.400	0.46	3.2
HSOG-D	0.226	11.5	0.391	0.49	2.19
HSOG-E	0.201	13.9	0.425	0.46	2.74
HSOG-F	0.189	12.5	0.330	0.40	1.64

* No AR coatings.

** AM1 simulation was a xenon source filtered by 7 cm of water.

*** Measured at 300 K.

TABLE II

Solar Cell Improvement Using d.c. Discharge Passivation

Honeywell Silicon-on-Ceramic Large Grained Material

	Best Result	Average Result
Air Mass One Efficiency - Virgin	2.7%	2.0%
Treated*	6.6%	4.9%
EBIC Dip, Virgin	26.09%	
Dip, Treated*	1.76%	
Ratio Treated/ Virgin	0.07	0.11
Isc Virgin	12.5 mA	14.4 mA
Treated*	25.5 mA	20.0 mA
Voc Virgin	.34 V	.39 V
Treated*	.47 V	.45 V

*Best treatment conditions: 1.125 torr H_2
2 min at 488°C 675 volts
2 min at 265°C 450 volts

References

1. D. Redfield, Appl. Phys. Lett. 40, 163 (1982).
2. B. W. Faughnan, J. Blanc, W. Phillips, and D. Redfield, Technical Progress Quarterly Report #3 for the period March 1980 - 24 June 1980, SERI/PR-0-8276-3, August 1980, p. 18.
3. N. M. Johnson, Bull. Am. Phys. Soc. 27, Abstract HB2, March 1982.
4. M. H. Brodsky and R. S. Title, Phys. Rev. Lett. 23, 581 (1969).
5. See for instance, "Defect Electronics in Semiconductors", by H. F. Matare, Wiley-Interscience (New York, 1971).
6. C. H. Seager and G. E. Pike, Appl. Phys. Lett. 35, 709 (1979).
7. C. H. Seager and T. G. Castner, J. Appl. Phys. 49, 3879 (1978).
8. Fundamental Studies of Grain Boundary Passivation in Polycrystalline Silicon with Application to Improved Photovoltaic Devices, C. H. Seager and D. S. Ginley, SAND81-1950, August 1981.
9. P. H. Robinson and R. V. D'Aiello, Appl. Phys. Lett. 39, 63 (1981).
10. R. T. Young, et al, Abstracts of the SERI Review Meeting for Polycrystalline Silicon Subcontractors, Washington, D.C., December 10, 1981.

Figure Captions

1. The zero-bias resistance of a grain boundary in as-received p-type Wacker Silso polysilicon plotted versus inverse absolute temperature.

2. Electron beam induced current (EBIC) map for a p-type Honeywell silicon on ceramic polysilicon sample, with a 0.3 - 0.5 micron diffused n-type layer. The area represented by the trace is approximately 0.01 cm^2. The total photocurrent is equal to the displacement between four horizontal traces. The upper trace is that for a sample annealed in vacuum prior to use. The lower trace is the same region (points "A" overlay) after d.c. treatment. Treatment conditions are 1.126 torr H_2; 5 mA - 650 V d.c., and 407°C for 20 min.

3. Spectrum A) polysilicon sample after 5 hr treatment at 590°C in 1.3 torr N_2 plasma 2 mA, 300 V sample polarity negative. Spectrum B) virgin polysilicon sample. Spectrum C) difference spectrum (A-B) after a 10 fold sale expansion showing the Si-N absorption. The position of this band indicates substoichiometric nitride formation and/or the presence of SiO.

4. Current-voltage data for a Honeywell p-type silicon on ceramic polycrystalline silicon sample with a diffused n-layer before and after d.c. plasma treatment. Treatment conditions were 1.125 torr H_2, 5 mA - 675 VDC, and 408°C for 2 minutes. Light intensity was 100 mW/cm^2, and an efficiency of 2.7%. The treated sample had Voc = 0.52 V, Isc = 22.0 mA/cm^2, and an efficiency of 6.3%. The cell area is ~1cm^2.

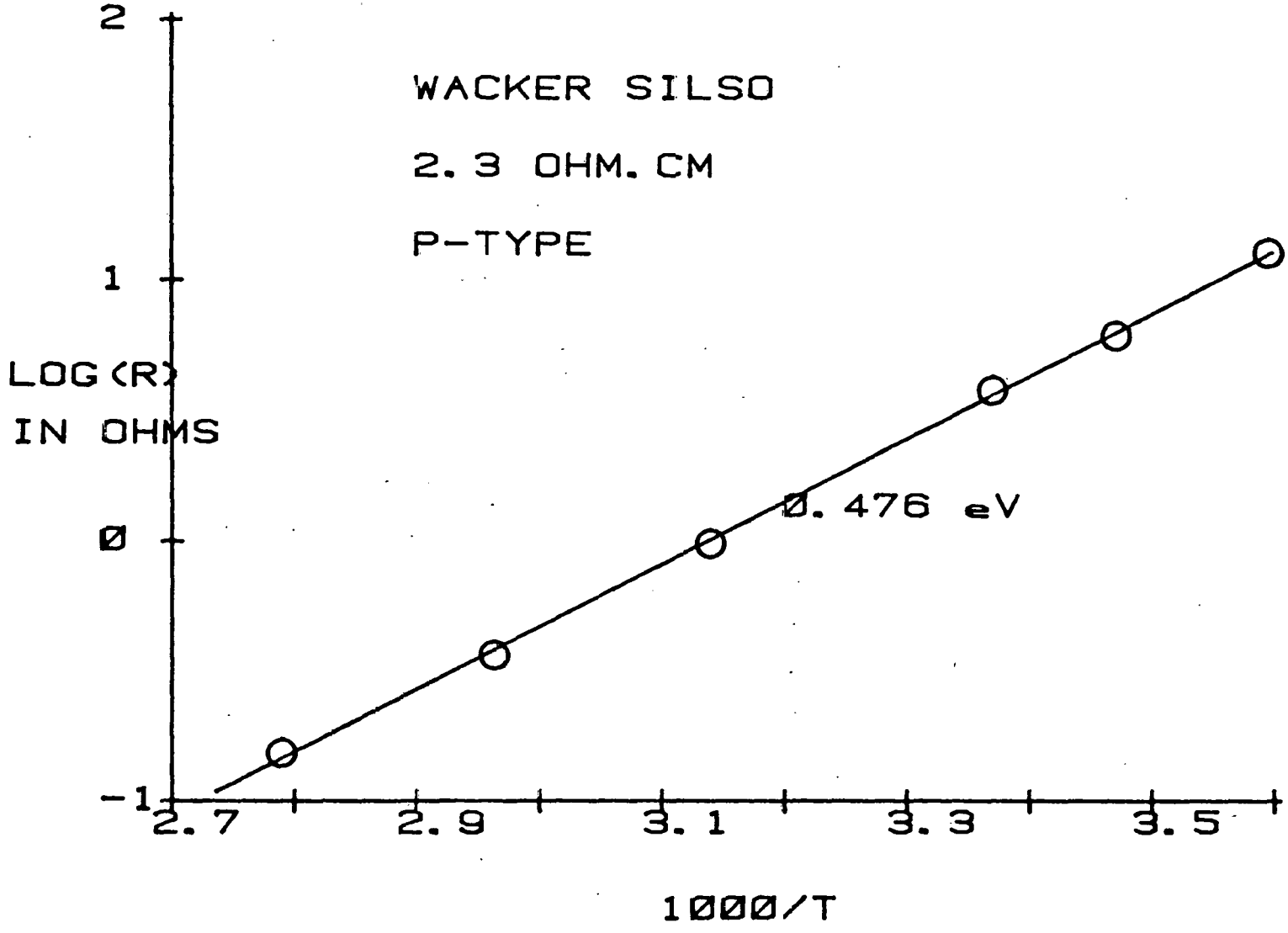
WACKER SILSO
2.3 OHM. CM
P-TYPE
0.476 eV
LOG(R)
IN OHMS
2
1
0
-1
2.7
2.9
3.1
3.3
3.5
1000/T

FIGURE 1

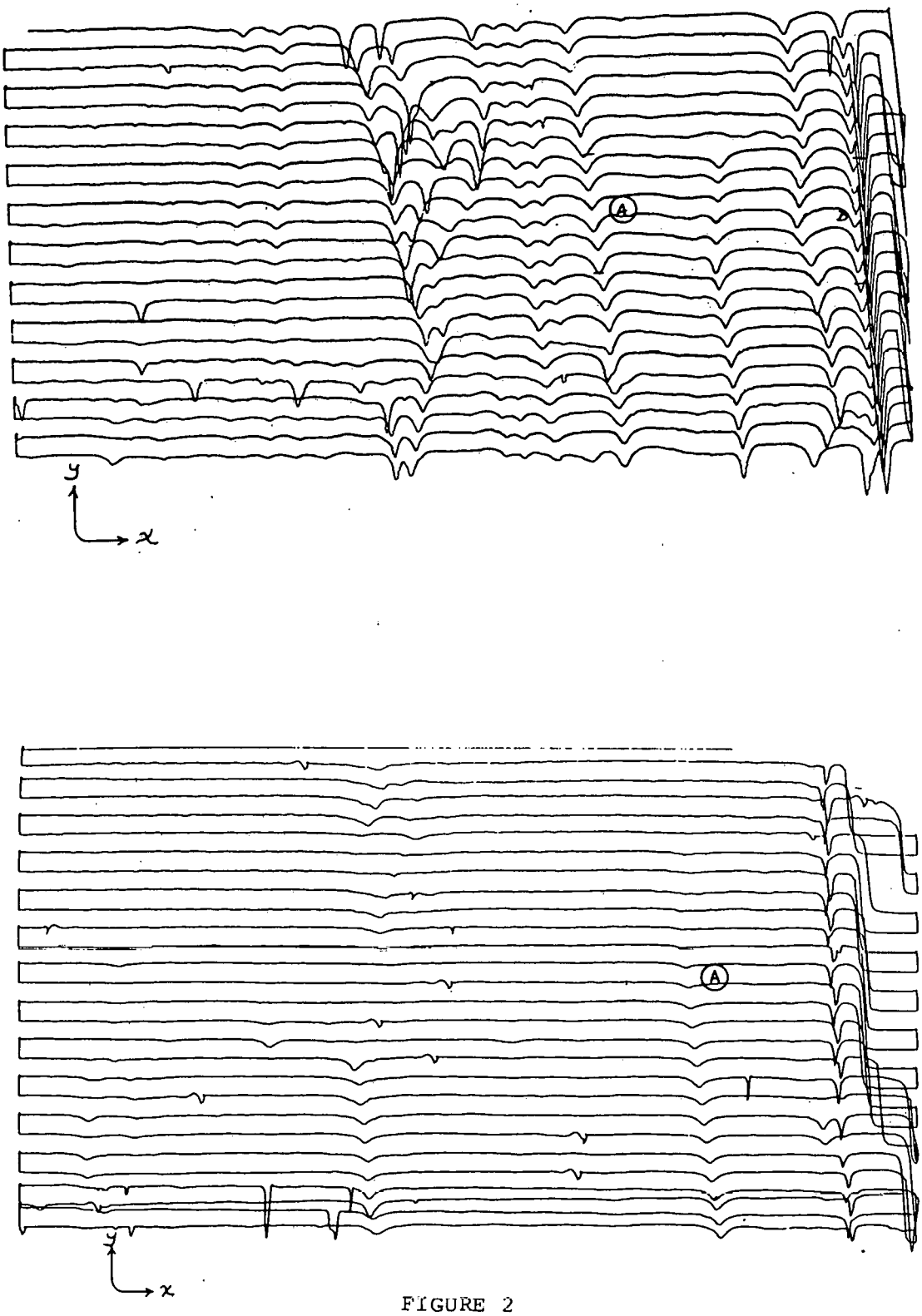

FIGURE 2

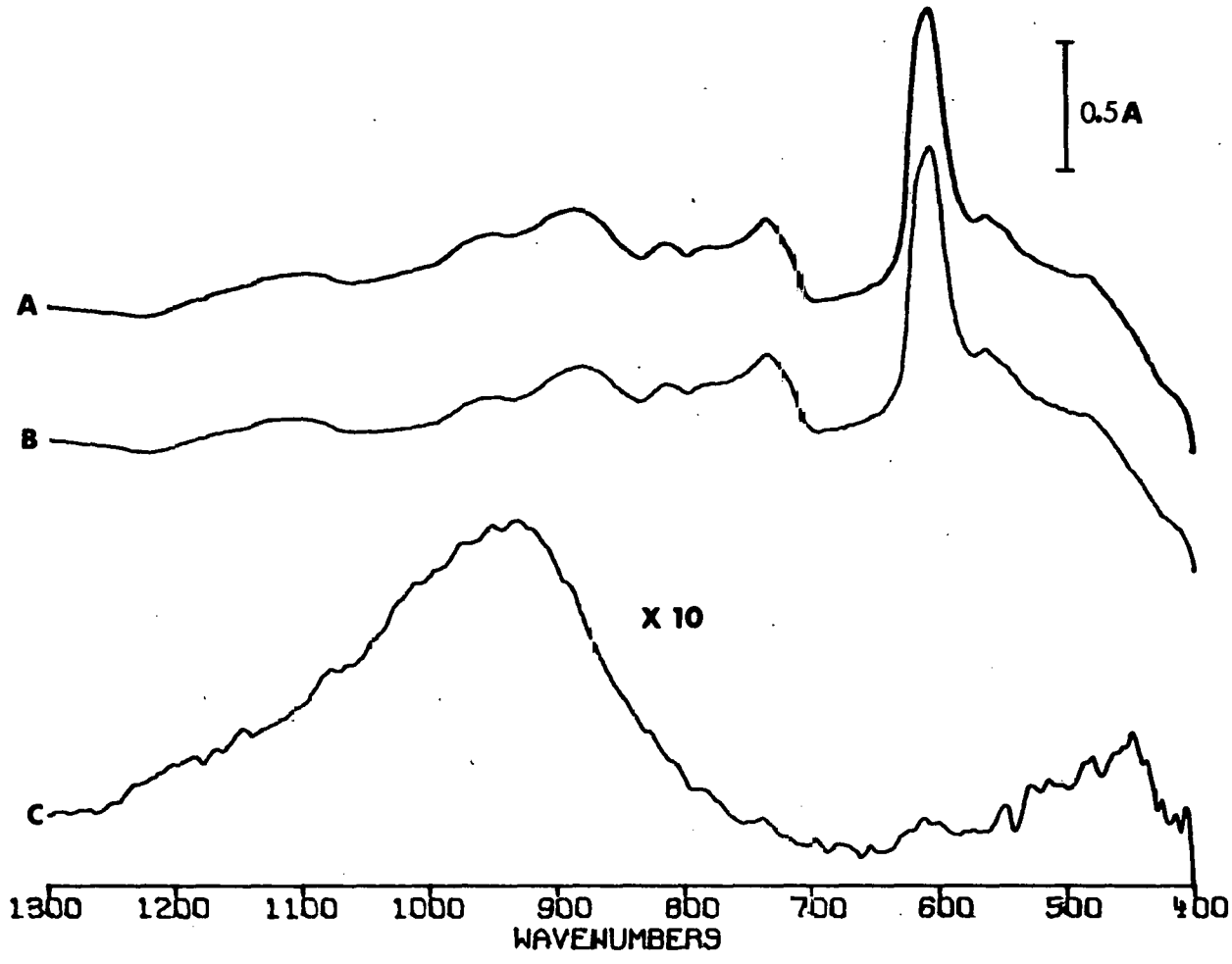
0.5A
A
B
X 10
C
1300
1200
1100
1000
900
800
700
600
500
400
WAVENUMBERS

FIGURE 3

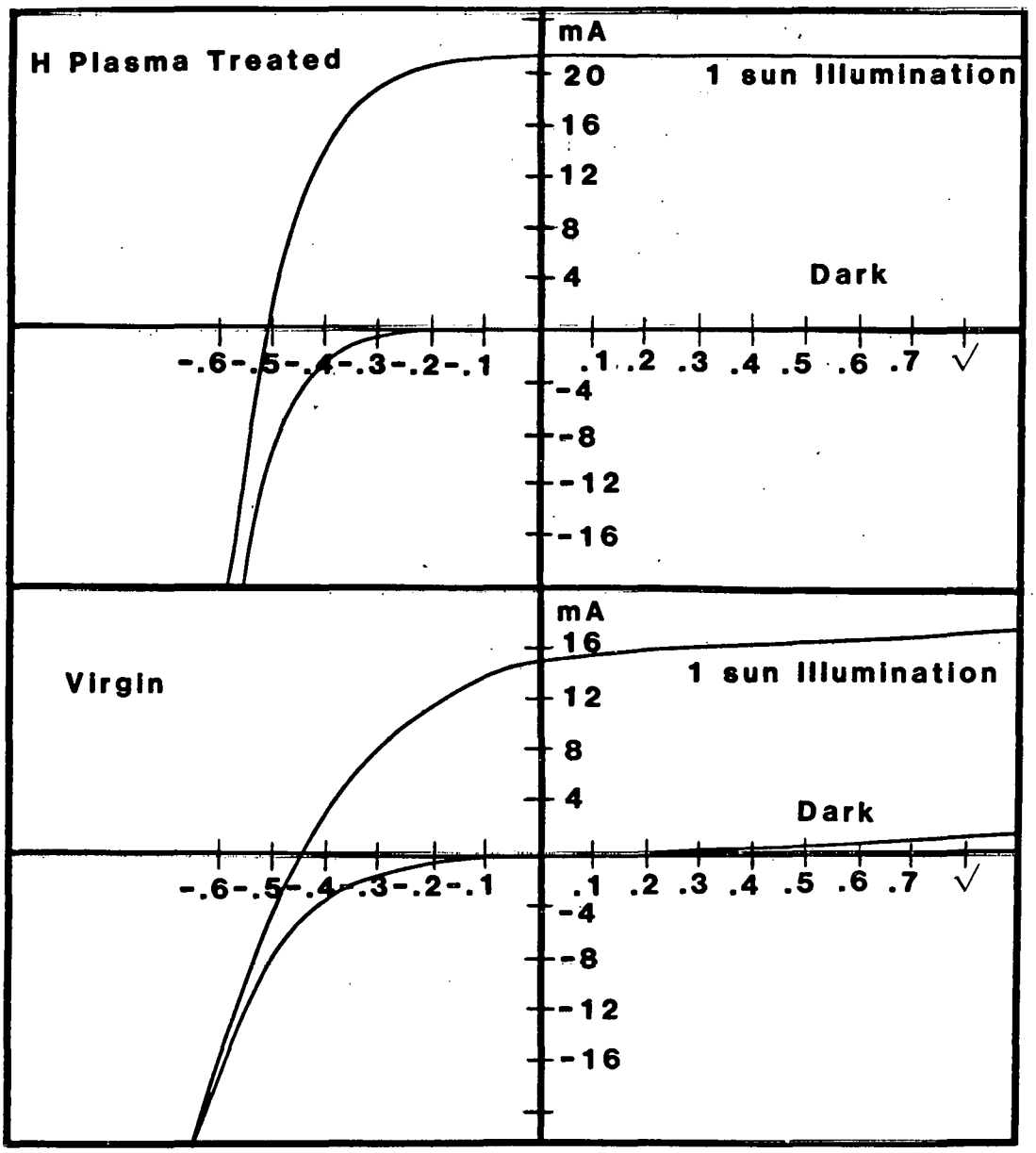
H Plasma Treated
mA
20
1 sun Illumination
16
12
8
4
Dark
-.6 -.5 -.4 -.3 -.2 -.1
.1 .2 .3 .4 .5 .6 .7 √
-4
-8
-12
-16
Virgin
mA
16
1 sun Illumination
12
8
4
Dark
-.6 -.5 -.4 -.3 -.2 -.1
.1 .2 .3 .4 .5 .6 .7 √
-4
-8
-12
-16

FIGURE 4

Appendices

A. The Passivation of Grain Boundaries in Silicon, C. H. Seager, D. J. Sharp, J. K. G. Panitz, and R. V. D'Aiello, J. Vac. Sci. and Technol. 20, 430 (1982).

B. Observation of Grain Boundary Hydrogen in Polycrystalline Silicon with Fourier Transform Infrared Spectroscopy, D. S. Ginley and D. M. Haaland, Appl. Phys. Lett. 39, 271 (1981).

C. Design of the high temperature, in situ, FTIR sample cell.

D. Modification of Grain Boundaries in Polycrystalline Silicon with Fluorine and Oxygen, D. S. Ginley, Appl. Phys. Lett. 39, 624 (1981).

Passivation of grain boundaries in silicon [a)]

C. H. Seager, D. J. Sharp, and J. K. G. Panitz

Sandia National Laboratories, [b)] Albuquerque, New Mexico 87185

R. V. D'Aiello

RCA Laboratories, Princeton, New Jersey 08540

APPENDIX A

(Received 14 August 1981; accepted 20 October 1981)

Several papers have demonstrated that the introduction of hydrogen into polycrystalline silicon can remove grain boundary trapping states. Evidence for this comes from studies of both majority carrier transport over grain boundary potential barriers and minority carrier recombination at these defects. Data on hydrogen passivation will be reviewed and the relative utility of both these transport measurements will be discussed with regard to the optimization of this process. Recent studies utilizing a Kaufman ion source have shown that increasing the proton energies and the dose rate greatly facilitates passivation in silicon. Simple diffusion models will be presented which account for these observations. This new treatment method has reduced the time necessary to improve photovoltaic cell parameters to the domain of commercial feasibility; the prospects for further improvements will be assessed. Because this passivation technique is essentially a low energy implantation process, there are accompanying damage and sputtering effects—methods for the control of these will be suggested.

PACS numbers: 61.70.Ng, 66.30.Jt, 73.60.Fw, 84.60.Jt

I. INTRODUCTION

In recent years our knowledge of the electronic structure and transport at semiconductor grain boundaries has grown considerably. This is particularly true in the case of silicon,[1] a material which has several applications of potential technological importance in its thin film (polycrystalline) form. Unfortunately, degradation of device properties by grain boundary effects can be quite severe in structures such as polycrystalline silicon solar cells[2] and thin film transistors.[3] Recent studies[4–7] involving the diffusion of atomic hydrogen into the grain boundary regions of silicon have shown that some, and perhaps all, of these degradation effects can be avoided with development of proper device processing procedures. The problem of optimizing this grain boundary passivation process and the evaluation of its effectiveness will be addressed in this paper. Our major emphasis will be on improving the efficiency of polycrystalline silicon photovoltaic cells and, hence, the improvement of minority carrier lifetimes near grain boundaries is our major concern. In other devices such as thin film MOSFETs where problems such as bombardment-damage induced surface states may be important, the types of treatment schedules discussed here may have to be followed by a damage removing etch step or other appropriate procedures.

The quantitative nature of the accumulation of excess majority carriers at grain boundaries has been recently studied in some detail.[8–12] We shall not attempt a review of this subject here. The basic phenomenon is that majority carriers trapped at grain boundary defect states form an attractive potential well for nearby minority carriers. This causes substantial recombination currents to flow toward the plane of the grain boundary.[13] For most boundaries, minority carriers impinging upon this plane almost never escape and hence can never be collected by the device junction as useful current. Photovoltaic collection efficiencies for fine grain ($< 100\,\mu$m) devices suffer accordingly. Other, equally detrimental effects occur due to the influence of grain boundaries on p/n (or other rectifying) junction properties in polycrystalline material. Under load, the total current in a photovoltaic device is the collected photocurrent minus the forward (dark) device current at the operating point. This latter current is large because of the effects of grain boundaries spanning the device junction. Generation-recombination currents due to in-gap grain boundary states in the junction region are a possible cause for this effect. Some modeling of this situation has been done,[14] but a full solution of the proper two-dimensional boundary value problem has not yet been published. In this work we shall concentrate strictly on the effects of grain boundaries on photogenerated minority carriers.

To what extent can we use the results of recent silicon bicrystal experiments to guide us in designing, optimizing, and interpreting grain boundary passivation experiments? Several distinct but related issues are involved. The first concerns our definition of the word passivation, itself. Initial experiments utilizing atomic hydrogen diffusion into silicon grain boundaries resulted in distinctly measurable increases in the conductance that these structures offered to majority carrier flow.[4,5] In the limit where tunneling is not important, the generally accepted form for this conductance (at zero bias) is[9,15,16]:

$$G_0 = (eA^{*}T/k)\, e^{-(\phi_B + \zeta)/kT}, \tag{1}$$

where ϕ_B is the height of the electrostatic potential barrier, ζ

is the separation of the Fermi level from the majority carrier band, and A^* is a pseudo-Richardson constant. It is easy to see that even small changes in ϕ_B can lead to substantial alternations of G_0; hence conductance measurements are very sensitive to the total amount of trapped charge Q in the grain boundary. Q varies as the square root of ϕ_B using a simple depletion approximation.[9,15] It is not hard to show that grain boundary barriers less than ~0.15–0.2 eV are very difficult to observe by conductance measurements at 300 K.[17] In fact, reduction of Q by a factor of two (obtained by treating with hydrogen, for instance) makes even high impedance grain boundaries "vanish" at 300 K, and one would hence be tempted to define the result as complete passivation. However, as we have observed in our laboratory,[17] such grain boundaries may still have very high minority carrier recombination velocities (hereafter designated as S). Recent theoretical calculations[13] have in fact indicated that barriers between 0.1 and 0.2 eV will have substantial ($> 10^4$ cm/s) values of S if the cross section of trapped majority carriers for capturing a minority carrier is typical of coulombic centers ($\sim 10^{-15}$–10^{-16} cm^2). Therefore, if we are truly interested in chemically improving polycrystalline material for a minority carrier device such as a solar cell, we should, in a straightforward fashion, define passivation in terms of a suitably low value of the grain boundary recombination velocity. Thus, only direct measurements of S appear to be appropriate in the optimization of any passivation process. The technique we shall employ here is that of scanned electron beam induced currents[18] (EBIC). Other techniques such as scanning light spot analyses (LBIC) are amenable to more quantitative estimates of S [19]; they also allow estimates to be made of passivation effects at larger distances (> 10 μm) from the collecting junction. We hope to employ LBIC measurements in the near future to complement our present studies.

While prior bicrystal studies give some direction as to the types of measurements which are necessary to define and optimize passivation in the context of photovoltaic devices, there is still a great deal that is unknown about the movement and bonding of hydrogen in polycrystalline silicon. Issues such as the primary mechanism for hydrogen diffusion in polycrystalline silicon (bulk or grain boundary), the nature of the Si–H environments, and the magnitude of the Si–H bonding energies for the important defect configurations are all subjects for future research. As a result, the present study has proceeded along largely empirical lines.

II. EXPERIMENTAL

A. The Kaufman ion source

Most of the previous H passivation studies performed in this laboratory have been done with a simple Tesla-coil induced plasma discharge. Although this apparatus is simple and inexpensive, the times required to substantially reduce grain boundary recombination are long,[6] and the control and measurement of ion energies and arrival rates is quite difficult.

The Kaufman ion source[20] represents an attractive alternative for treating polycrystalline silicon with hydrogen (or other) ions. These machines are commercially available and are apparently amenable to scaling to quite large sizes. Furthermore, the peak ion energies and currents are readily controllable and measurable. Other simple and effective dc discharge plasma generators are under investigation in this laboratory,[17] but results from these will not be discussed here.

The apparatus used in the present studies is a Veeco "Microetch System."[21] The rather uniform ($\pm$ 10%) ion beam[22] produced by this machine strikes the sample(s) resting on the target area, which in our case is primarily silicon to prevent surface contamination by sputtered target material. Sample temperature is monitored by a thermocouple imbedded in the temperature controllable target base. Some ion bombardment heating of the sample and base occurs at the power densities used during these experiments (up to 2 W/cm^2). The sample chamber is oil diffusion pumped with a system of the same manufacture.

It is important to note that the Kaufman Source beam consists of several species: H, H^+, H_2^+ and is not strictly monoenergetic.[22] We discuss this further in Sec. III.

B. Sample preparation

Several types of polycrystalline silicon devices were used in the course of this study. All were n^+/p diodes with grain boundary planes primarily perpendicular to the collecting junction. The devices used in the EBIC measurements and for the quantum efficiency measurements were grown at the Honeywell corporation.[23] These were of two types: the first (hereafter called SOC) was a mullite ceramic substrate with a ~250-μm-thick polycrystalline silicon layer produced by dip coating in a crucible of molten silicon.[24] The base doping level in these samples was about 2×10^{16} cm^{-3} (boron) and junction formation was via phosphorous diffusion at 850 °C. The back metallization was sintered platinum; no front grids were needed due to the low currents drawn in the EBIC measurements. Silver paint was used to contact the ~0.3-μm-thick emitter layer. A similar Honeywell material was used for the quantum efficiency measurements discussed in Sec. IIIB.—the difference being the use of a high-purity graphite layer as the substrate. This material (called SOG) had grain sizes of the order of 75 μm vs the 300–500 μm of the SOC samples. Base doping and junction parameters were similar to those for the SOC samples.

Fully gridded polycrystalline silicon solar cells grown at the RCA Laboratories were used for the white light measurements described in Sec. IIIB. These devices had a 20-μm-thick epitaxial silicon layer grown by CVD processing at 1150 °C on a DOW Corning upgraded metallurgical grade (2P) polycrystalline silicon substrate. Base doping in the epilayer was $\sim5\times10^{16}$ cm^{-3} (boron), and the emitter was formed by a standard phosphorous diffusion. The front grid structure was of a standard parallel finger design using Ti/Ag metallizations. No antireflection coatings were present in order that the hydrogen processing steps could be properly implemented.

C. EBIC studies

The circuitry for accomplishing EBIC studies uses a Motorola MC6800 microprocessor to control the X and Y posi-

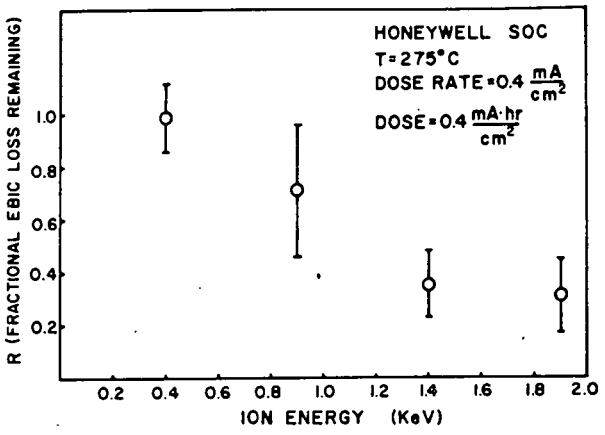

FIG. 1. The EBIC contrast ratios (after/before) of several grain boundaries following Kaufman ion source treatments of Honeywell n^+/p SOC polysilicon diodes at various peak ion energies. The dose, dose rate, and sample temperature were fixed for these experiments.

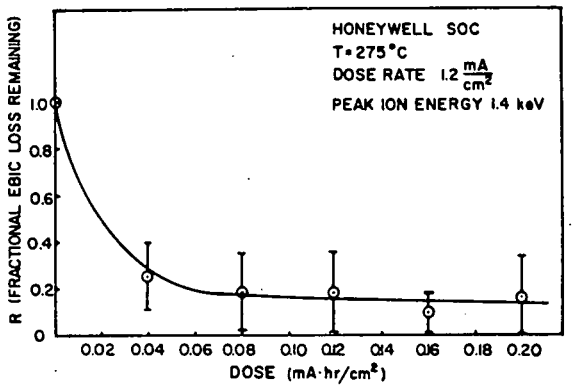

FIG. 3. The EBIC contrast ratios (after/before) of several grain boundaries following Kaufman ion source treatments of Honeywell n^+/p polycrystalline silicon diodes as a function of total ion dose. The other passivation parameters were fixed during this series of experiments.

tions of both the electron beam of an ISI Mini-SEM Series II microscope and the pen of an X–Y plotter. A detailed description of this apparatus is available elsewhere.[17] From the published literature[18,25] and our own experiments, we believe that the diameter of the region of electron-hole pair generation is ~6–8 μm at our beam energy (25 kV). The distribution of excess carriers is not uniform however, and depends to a significant extent on the minority carrier recombination velocity at the surface of our samples as well as on the bulk lifetime.[18] When the electron beam is brought into the vicinity of a grain boundary surface normal to the collecting junction (characterized by a recombination velocity S), a reduction in short circuit collected circuit, I_{sc}, is observed. The peak value of this loss, when normalized by the bulk photocurrent is sometimes called the EBIC contrast. In principal, if sufficiently accurate values of the surface, bulk, and p/n junction parameters were known, the actual shape of I_{sc} vs distance plots could be used to estimate S. In practice, however, this is very difficult and we prefer to ignore the issue of the exact values of S and use the ratio of EBIC contrasts in the treated/virgin state to define an index of passivation (labeled R, in Figs. 1–3). For our diodes, the grain boundary EBIC contrast values are typically 0.25–0.35 before treatment. After an optimized passivation schedule they typically fall to 0.05 or less.

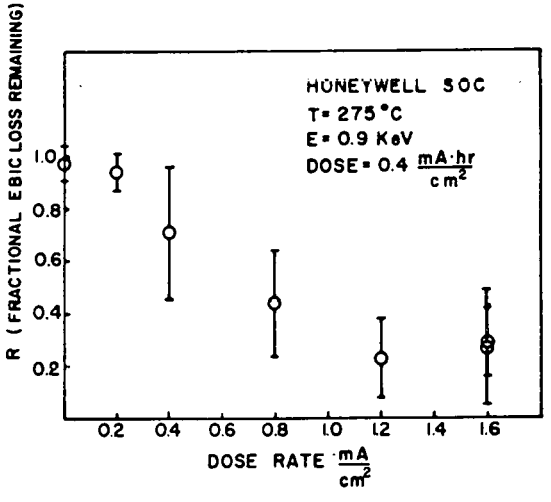

FIG. 2. The EBIC contrast ratios (after/before) of several grain boundaries following Kaufman ion source treatments of Honeywell n^+/p polycrystalline silicon diodes at various ion dose rates. The dose, peak ion energy, and sample temperature were fixed.

Several cautions should be observed in interpreting EBIC data. The first is that alterations of the free surface recombination velocity could in principal affect these measurements.[18] Because the hydrogen ion beam does damage to the surface of the sample, some change in the surface recombination currents is likely; but based on some ancilliary experiments, we do not feel that these effects are of substantial importance. The second issue which could be of concern is whether the surface and grain boundary recombination velocities are functions of the excitation levels employed here; in this case, deliberate variations of the exciting beam intensity should change the character of EBIC plots. We have looked for this effect several times and have not observed it. There are in fact theoretical reasons to believe that, for barrier heights typical in p-type silicon doped in the 10^{16}–10^{17} cm^{-3} range, grain boundary recombination velocities are likely to be independent of excitation level for the beam currents (typically 1 nA) used in our SEM.[13] With these provisos then, we take the ratio of EBIC contrasts as a useful, quantitative measure of the efficacy of passivation.

III. RESULTS

A. Optimization

The independently variable ion bombardment parameters in these experiments include ion energy, dose, dose rate, and sample temperature. For this reason, a complete evaluation of the entire matrix of possible treatment conditions would be an imposingly lengthy task. This is particularly true in light of the fact that the grain boundaries in the material that we have studied show a variety of behavior upon exposure to hydrogen—we have tried to compensate for this problem by examining many boundaries and averaging the results. The

data shown here is in some sense preliminary because a more detailed study involving thorough variation of the passivation parameters is just beginning. In many cases, the present data were obtained by fixing all but one of the parameters in a region where encouraging results were forthcoming, while varying the remaining one. Deducing an optimum set of passivation conditions from this procedure involves assuming that there are no parametric interactions between these parameters. In lieu of any more detailed data which might suggest the contrary, we adopt this assumption.

Figures 1–3 show plots of the EBIC contrast ratio ($\simeq$ maximum I_{sc} loss at the grain boundary after treatment/before treatment) for variation of three treatment parameters: peak ion energy, dose rate, and dose. All data were obtained on Honeywell SOC n^+/p diodes and each point represents an average of the behavior of at least 10 grain boundaries measured at several points along their intersection with the sample surface. The abscissa of Fig. 1 should be interpreted strictly as the *peak* energy in the ion spectrum. The actual ion energy distribution has a substantial tail at energies less than the peak,[22] and the population in this tail grows with peak ion energy. This smearing effect is quite pronounced when operating this ion source with light ions.

The tendency for more complete passivation for higher ion energies and dose rates (currents) is quite evident in Figs. 1 and 2. It suggests that our previous implicit assumption[7,17] that the exposed silicon surface was saturated with hydrogen during our Tesla-coil plasma hydrogenation experiments was far from correct. A one-to-one correlation of hydrogen ion fluxes between the Kaufman source and our prior apparatus[7,17] is difficult, but these results, as well as the data in the following section, suggest that the ion arrival rates and energies are considerably larger in the present case. While the efficacy of supplying ions at higher rates is rather obvious if diffusion into the bulk is fast enough to deplete the near surface hydrogen concentration, the beneficial effect of raising the ion energy is not so easily anticipated. We defer discussion of this effect to Sec. IV.

The dependence of passivation efficiency on ion dose is shown in Fig. 3. This type of curve is not uncommon for a process which is an ideal sense is presumably proceeding towards some final equilibrium state. There are practical difficulties in exposing samples to large enough doses to determine whether this equilibrium state is one where all boundaries are completely passivated (no current loss). Aside from the boundary-to-boundary scatter evident from the error bars in Figs. 1–3, a true equilibrium measurement is difficult to make due to the nonnegligible rate of silicon removal at the higher ion energies and current rates.[22] From calibration runs[22] we estimate that we are sputtering off about 4500 Å/h at 1.0 keV and 1.2 mA/cm^2. This means that very long passivation runs will remove all of the heavily doped n^+ layer in our Honeywell diodes. Further discussion of this point appears in Sec. IV.

Several considerations affect the choice of the remaining treatment parameter which is the sample temperature. Because either grain boundary or bulk diffusion would be expected to proceed more rapidly at elevated temperatures, we have only investigated the regime of sample temperatures above 25 °C. It is important to note that data exist which indicate that significant debonding of hydrogen occurs above ~375 °C. Outgassing of diffused-in D/H mixtures in polycrystalline silicon has been seen[17] above 375 °C in our prior gas analysis studies. In addition, vacuum anneals above 400 °C have also been observed to depassivate H-treated silicon grain boundaries in recent EBIC measurements.[17] Because of these facts, we have not included sample temperatures above 375 °C in our initial studies. These experiments have concentrated in the 200–350 °C range and seem to show a weak maximum in the passivation effect in the region of 250–300 °C. The overall variation in this range is not large, however, particularly when compared to the type of boundary-to-boundary spread indicated by the error bars in Figs. 1–3. As in the case of the other parameters, investigation of more detailed variations is underway.

B. Applications

Although the primary purpose of this paper is to present and discuss hydrogenation optimization data, our eventual goal is the processing of polycrystalline silicon solar cells for operation in AM1 sunlight. Demonstration of the effects of this passivation process on the white light performance of several types of structures has recently begun in our laboratory and some preliminary results of these studies are detailed below.

One such study is the production of a prototype polycrystalline silicon cell which has low enough impurity levels and small enough grains to insure that grain boundary effects are the *primary* cause of efficiency degradation. Theoretical considerations suggest that in order to lose a significant fraction of short circuit current to grain boundary recombination, the average grain size should be not much bigger than, say, 5× the thickness where most of the AM1 light is absorbed. This rough rule of thumb indicates that silicon cells with grain sizes less than ~100 μm will be quite seriously affected by recombination losses. Degradation of dark I–V properties should also be expected to be serious at this grain size level,

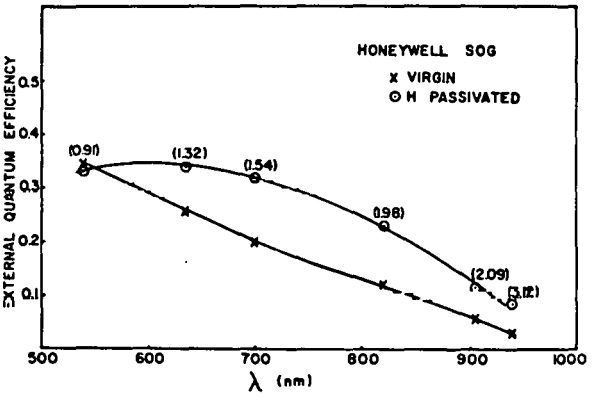

FIG. 4. The external quantum efficiency (uncorrected for reflection) vs wave length for a Honeywell silicon-on-graphite n^+/p diode before and after hydrogen passivation at 1.4 keV, 1.2 mA/cm^2 at 325 °C for 20 min. The numbers in parentheses are the ratios of the after and before treatment efficiencies.

TABLE I. The AM1 solar cell parameters of several non-AR coated RCA epitaxial solar cells. AM1 simulated light was a xenon source filtered by 7 cm of water. H passivation was in the Kaufman Ion Source at 275 °C, 1.4 keV, 1.2 mA/cm² for 2 min. Numbers in parentheses are estimates of current and efficiency if the cell reflectivity had not changed (see text).

Cell #	Type	Treatment	I_{sc} (mA/cm²)	V_{oc}	ff	eff (AM1)
1	Single crystal	Virgin	20.3	0.57	0.72	8.3%
1	Single crystal	H passivated	23.3 (21.9)	0.57	0.70	9.3 (8.7)
2	Polycrystal	Virgin	19.3	0.51	0.62	6.1
2	Polycrystal	H passivated	22.5 (21.1)	0.55	0.73	8.3 (7.8)
3	Polycrystal	Virgin	20.0	0.52	0.63	6.5
3	Polycrystal	H passivated	20.5 (19.3)	0.55	0.73	8.2 (7.7)
4	Polycrystal	Virgin	19.3	0.52	0.70	7.0
4	Polycrystal	H passivated	21.5 (20.2)	0.55	0.71	8.4 (7.9)

since these effects are quite noticeable for even 1 mm grain size cells (see below).

The Honeywell SOG silicon described in Sec. II.B appears to be a good candidate for the substrate of this demonstration cell. To get a feeling for the hydrogen-induced changes we might expect from cells made on this material, we have begun to fabricate n^+/p structures by using phosphorous ion implantation to form the n^+ layer. The quantum efficiency of one of these devices is shown in Fig. 4 at several wave lengths. This diode has no top metallization and no AR coating and can only produce small photocurrents without series resistance problems. The response of the virgin diode falls off drastically in the infrared but improves significantly after hydrogenation. We infer from these changes that white light photocurrent would show substantial gains at AM1. EBIC maps of such diodes show large reductions in grain boundary losses, and thus it is reasonable to conclude that the changes seen in Fig. 4 are primarily grain boundary related. Fabrication of fully gridded AM1 devices on these substrates is underway.

The second type of cells we shall discuss were fabricated at RCA laboratories on much larger grained (~1 mm) silicon. As can be seen from examination of Table I, the primary differences between these cells and those made by the same processing on single crystal silicon wafers is the presence of poorer diode characteristics (V_{OC} and fill factor). Thus, even at these grain size levels, the presence of polycrystallinity has important effects. Recently,[26] low pressure hydrogen plasma discharge treatment of similar cells for 4 h at RCA Laboratories has been shown to improve AM1 efficiencies by ~10%. After only 2 min of hydrogenation with the Kaufman source, fill factors and open circuit voltages are as significantly improved as in this prior study. There are also gains in short circuit current, but some of these are due to a measurable decrease (~15% in white light) in the specular reflection of the treated cell surface. This effect is a curious by-product of the ion bombardment and suggests that significant stoichiometry changes occur at the treated surface.

IV. DISCUSSION

EBIC data of the type presented in Sec. IIIA., while useful in optimizing the grain boundary hydrogenation process, do not permit much insight to be drawn into the nature of the physics involved. Certain aspects of this data, particularly the ion energy dependence shown in Fig. 1, are rather puzzling at first glance. If we make the conceptual leap of identifying a small value of the remaining EBIC loss, R, with the existence of large concentrations of hydrogen well below the surface (several microns) during the treatment, we can attempt to model the hydrogen diffusion process and ascertain why it should depend on ion energy.

The most obvious parameter that scales with ion energy is the ion penetration distance. This is a roughly linear function of ion energy and is of the order of ~400 Å at 1.5 keV for protons in silicon.[27] If we now write down a very simplified diffusion equation for $c(x,t)$, the concentration of hydrogen, assuming a roughly distance independent ion deposition rate, r, from the surface (at $x = 0$) to some depth, x_p, we have:

$$\frac{\partial c(x,t)}{\partial t} = D\frac{\partial^2 c(x,t)}{\partial x^2} + r(x), \tag{2}$$

where $r(x) = r$ (a constant) for $0 < x < x_p$

$= 0$ for $x > x_p$

and D is the diffusion coefficient of hydrogen in silicon. r is a function of the ion current and the penetration distance x_p as expressed by

$$rx_p = I/e, \tag{3}$$

where I is the ion current in A/cm², and e is the electronic charge. In attempting to define the boundary conditions for solution of this problem, a reasonable assumption to make is that any hydrogen which diffuses back up to the surface of the sample can readily escape, i.e.,

$$c(0,t) = 0. \tag{4}$$

The solution to Eq. (2) under these conditions is[28]:

$$c(x,t) \simeq \left[\frac{Ix_p}{2eD}\right] \operatorname{erfc}\left(\frac{x}{\sqrt{4Dt}}\right), \tag{5}$$

for $x > x_p$ and $x_p < 2\sqrt{Dt}$. Considering the magnitude of x_p, the latter restriction is probably well satisfied in the cases we are interested in. Equation (5), through the explicit ion energy dependence of x_p, provides a straightforward explanation for why hydrogen diffusion might be more effective at higher ion energies. Basically, the deeper an ion is implanted in the material, the more chance it has of diffusing into the bulk rather than back to the free surface. Of course, the dose rate dependence of $c(x,t)$ is also evident in Eq.(5). At high enough

dose rates, the factor in square brackets in this equation will approach the saturation concentration of hydrogen in silicon—a number which one might estimate at between 10 and 40 at.% from prior work in this area.[29] At this point the assumptions of the model are rather suspect, and it is unclear what physical behavior to expect. Even before this point, a significant concentration dependence of D will undoubtedly become important. We admit that the entire issue of modeling the diffusion of a species in a damaged region undergoing constant ion bombardment is a difficult one at best. The point of the present model is to give the simplest rationale for expecting results such as those in Figs. 1 and 2.

Although the diffusion equation written above was given in a one-dimensional form, this was not based on any concrete information about the importance of bulk vs grain boundary hydrogen diffusion. Extended extrapolation of high temperature bulk H diffusion coefficients in single crystal silicon[30] results in numbers which are still high enough at 200–300 °C to account in a qualitative way for some of the prior hydrogenation results that we have obtained. The validity of this extrapolation is questionable, however, and hard data on hydrogen diffusion in single and polycrystalline silicon is needed in this temperature range.

It is worth pointing out that there are two effects which are inevitable after irradiation of a material with energetic ions: radiation damage and material removal. The former may have serious effects on the surface recombination velocities in a solar cell structure—the decrease in the quantum efficiency at 540 nm in Fig. 4 may be evidence for this. Because of the rather low temperatures required to thermally depassivate hydrogenated grain boundaries, thermal annealing of this damage is probably out of the question. Chemical etching to remove this layer is a possibility, however. Protecting a silicon surface from being sputtered during hydrogen bombardment is an easier task—metal overlayers could be effective in this regard. We have successfully hydrogenated n^+/p diodes which had a ~80-Å-thick overlayer of deposited tungsten. The sputtering rate of tungsten by hydrogen is very low, and the efficiency of the hydrogenation process does not seem to be drastically impaired.

Aside from the many unknowns in this process, the conclusion that hydrogen removes many if not all of grain boundary trapping states in silicon is inescapable. Whether or not this process will permit thin film silicon cells to approach 10% AM1 efficiency is still a matter of conjecture. It is obvious, however, that more understanding of the detailed physics in this area is needed. Given this understanding, we can expect further improvements in the speed and effectiveness of the grain boundary hydrogenation process.

ACKNOWLEDGMENTS

The authors would like to thank L. N. Rapp for his assistance in the EBIC measurements and P. S. Peercy and J. Clement for the ion implantation and annealing steps on the Honeywell SOG diodes. D. K. Brice provided useful data and discussions on the nature of the hydrogen implantation process in silicon, and J. D. Zook of Honeywell Corporation graciously supplied the Honeywell SOC and SOG material.

[a]This work was sponsored by the U.S. Department of Energy (DOE) under Contract DE-AC04-76-DP00789

[b]A U.S. Department of Energy facility

[1]G. E. Pike and C. H. Seager, Adv. in Ceramics **1**, 53 (1981).

[2]See, for example, T. L. Chu, S. S. Chu, K. Y. Duh, and H. I. Yoo, in *Proceedings of the National Workshop on Low Cost Polycrystalline Silicon Solar Cells*, May 18–19, 1976, Dallas, TX, p. 408.

[3]J. C. Anderson, Thin Solid Films **37**, 127 (1980).

[4]C. H. Seager and D. S. Ginley, Appl. Phys. Lett. **34**, 537 (1979).

[5]D. R. Campbell, M. H. Brodsky, J. C. M. Hway, R. E. Robinson, and M. Albert, Bull. Am. Phys. Soc. **24**, Abstract JK 3 (1979).

[6]C. H. Seager, D. S. Ginley, and J. D. Zook, Appl. Phys. Lett. **36**, 831 (1980).

[7]C. H. Seager and D. S. Ginley, J. Appl. Phys. **52** (2), 1050 (1981).

[8]C. H. Seager and T. G. Castner, J. Appl. Phys. **49**, 3879 (1978).

[9]G. E. Pike and C. H. Seager, J. Appl. Phys. **50**, 3414 (1979).

[10]C. H. Seager and G. E. Pike, Appl. Phys. Lett. **35**, 709 (1979).

[11]C. H. Seager, G. E. Pike, and D. S. Ginley, Phys. Rev. Lett. **43**, 532 (1979).

[12]C. H. Seager and G. E. Pike, Appl. Phys. Lett. **37**, 747 (1980).

[13]C. H. Seager, J. Appl. Phys. **52**, 3960 (1981).

[14]J. G. Fossum and F. A. Lindholm, IEEE Trans. Electron Devices ED-27, 692 (1980).

[15]W. E. Taylor, N. H. Odell, and H. Y. Fan, Phys. Rev. **88**, 867 (1952).

[16]R. K. Mueller, J. Appl. Phys. **32**, 635 (1961); **32**, 640 (1961).

[17]C. H. Seager and D. S. Ginley, *Fundamental Studies of Grain Boundary Passivation with Application to Improved Photovoltaic Devices*, Sandia National Laboratories Report #SAND80-2461, August 1980.

[18]For an excellent review of this subject see H. J. Leamy, in *Physical Electron Microscopy*, edited by O. C. Wells, K. F. J. Heinrich, and D. E. Newbury (Van Nostrand Reinhold, New York, 1981).

[19]J. D. Zook, Appl. Phys. Lett. **37**, 223 (1980).

[20]H. R. Kaufman, J. Vac. Sci. Technol. **15**, 272 (1978).

[21]Veeco Instruments Inc., Terminal Drive, Plainview, N. Y., 11803.

[22]For a discussion of Kaufman ion source beam composition and uniformity see: D. J. Sharp, J. K. O. Panitz, and D. M. Mattox, J. Vac. Sci. Technol. **16**, 1879 (1979).

[23]Provided by J. D. Zook.

[24]See, for example: J. D. Zook, S. B. Schuldt, R. B. Maciolek, and J. D. Heaps, in *Proceedings of the Thirteenth IEEE Photovoltaic Specialists Conference* (IEEE, New York, 1979) p. 472.

[25]N. Inoue, S. M. Goodnick, and C. W. Wilmsen in *Proceedings of the Thirteenth IEEE Photovoltaic Specialists Conference* (IEEE, New York, 1979), p. 472.

[26]P. H. Robinson and R. V. D'Aiello, Appl. Phys. Lett. **39**, 63 (1981).

[27]D. K. Brice (private communication).

[28]H. S. Carslaw and J. C. Jaeger, *Conduction of Heat in Solids* (University of Oxford, Oxford, 1959), p. 79.

[29]I. I. Pankove, M. A. Lampert, and M. L. Tarng, Appl. Phys. Lett. **32**, 439 (1978).

[30]*Fundamentals of Silicon Integrated Device Technology*, edited by R. M. Burgerand, R. P. Donovan (Prentice-Hall, Englewood Cliffs, NJ, 1967), Vol. 1.

Observation of grain boundary hydrogen in polycrystalline silicon with Fourier transform infrared spectroscopy[a)]

D. S. Ginley and D. M. Haaland
Sandia National Laboratories,[b)] Organization 5154, Albuquerque, New Mexico 87185

APPENDIX B

(Received 16 March 1981; accepted for publication 1 May 1981)

Fourier transform infrared spectroscopy has been applied to the study of polycrystalline silicon samples previously exposed to rf- and dc-induced hydrogen plasmas. The first direct observation of hydrogen incorporated in the grain boundaries has been made. Peaks attributable to surface hydrogen have also been observed. The techniques developed show considerable utility in probing the very small numbers of impurity atoms in grain boundaries.

PACS numbers: 78.30.Gt, 81.40.Tv, 84.60.Jt, 73.20.Hb

Thin films of polycrystalline silicon have received considerable attention as potential photovoltaic solar converters. While deposition costs for these films are economically attractive, device efficiencies historically have been too low to make the devices practicable. One of the chief factors responsible for the reduced efficiency is the detrimental nature of the grain boundaries.[1] Recently, considerable progress has been made in understanding the electronic structure of silicon grain boundaries.[2-5] It has also been demonstrated[6-8] that the diffusion of monatomic hydrogen into polycrystalline silicon is capable of removing grain-boundary trapping states, as implied from zero-bias grain boundary impedance measurements.[2] This technique can remove (at 300 K) all grain boundary potential barriers to depths greater than 0.5 mm in silicon.[9] In addition, it has been demonstrated that hydrogenation of polycrystalline silicon can substantially reduce minority-carrier recombination at grain boundaries and significantly improve p/n junction quality.[10]

To fully optimize the grain-boundary passivation techniques, it is extremely useful to develop an understanding of the chemical and structural nature of the hydrogen in the silicon grain boundaries. A considerable literature exists on the nature of hydrogen in amorphous and single-crystal silicon as studied by infrared spectroscopy.[11-16] Owing to the very small amount of impurity atoms incorporated even in fine-grain polycrystalline silicon (about 10^{14} atoms/c.c. or less), conventional techniques are incapable of readily probing grain-boundary impurities. For the first time using the enhanced sensitivity of Fourier transform infrared spectroscopy (FT-IR),[17] we have been able to detect and identify Si-H vibrations arising from hydrogen located in the grain boundaries and on the surface of the silicon samples after they have been exposed to hydrogen plasmas.

The polycrystalline silicon samples employed in the present study were Texas Instrument's fine-grain, chemical vapor deposited, semiconductor-device-grade silicon. Typical grain sizes in the material are 25-50 μm. Doping was via the neutron transmutation method; the radiation damage incurred during the process was annealed out *in vacuo* at 800 °C for 1 h. The doping level was 2×10^{14} P/cm^3 or below. The sample configuration employed was a polished (1/4 μm diamond grit) parallelpiped $0.5 \times 1.0 \times 0.1$ cm^3. Single-crystal silicon employed as a reference was Monsanto (100) silicon neutron transmutation doped to 8×10^{14} P/cm^3 or less.

Plasmas were produced either by rf (tesla coil) or by a dc two-plate apparatus as previously described.[9] If a dc plasma was employed, the silicon was always in contact with the negative plate. All treatments were run on samples etched for 10 min in 10% HF to remove surface oxide. Treatment parameters were at the values which passivated the grain boundaries as determined previously from zero-bias grain-boundary impedance measurements. These were 0.5-2-Torr H_2, 350-500 °C, and 24-65 h for rf plasmas; and 5.0-Torr H_2, 450 °C, 10 mA, and 1-2 h for dc plasmas. All anneals were done in vacuum (5×10^{-7} Torr) and at temperatures between 600 and 850 °C as specified. All etches, other than surface HF etches, utilized Sirtl etch $CrO_3/HF/H_2O$.

All infrared spectra were run at room temperature on a Nicolet 7199 FTIR spectrometer equipped with a liquid-N_2-cooled InSb detector. In order to obtain sufficient signal-to-noise levels to observe the small Si-H absorptions, spectra from 5000 to 1850 cm^{-1} with 4 cm^{-1} resolution were obtained by signal averaging 1000 interferograms. The spectrometer was purged with dry N_2 to eliminate interfering absorption from water vapor. By mounting the samples on a remotely operated linear motion translator, spectral backgrounds could be taken through the same optical path without breaking the spectrometer purge. The base lines of the spectra presented in this report have been corrected by subtracting linear base lines over the spectral region containing the Si-H stretching vibrations.

Figure 1 illustrates a spectrum of the Si-H stretching region for polysilicon and single-crystal silicon samples before and after H-plasma treatment. A number of new peaks are observed in each case. The peak at 2019 cm^{-1}, which is reproducible in position and spectral linewidth, is unique to the hydrogenated polycrystalline silicon sample. The broad peaks at ~2115 and 2105 cm^{-1} in the single and polycrystalline samples, respectively, are not highly reproducible in peak frequency, intensity, and linewidth. These bands could be associated with either surface or bulk SiH_x bonds. In order to differentiate between these possibilities and to confirm the origin of the 2019-cm^{-1} peak as due to grain-boundary hydrogen, the samples shown in Fig. 1 underwent a

[a)]This work was supported by the U.S. Department of Energy under Contract DE-AC04-76-DP00789.

[b)]A U.S. Department of Energy facility.

 0003-6951/81/150271-03$00.50

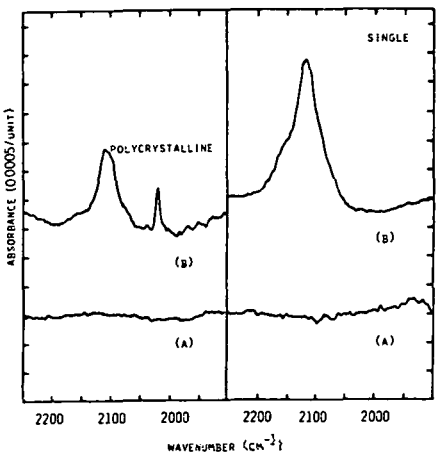

FIG. 1. Fourier transform infrared spectra of the Si-H stretching region for a polycrystalline and a single-crystal silicon sample after (A) 800 °C anneal for 1 h in vacuum and (B) after two 16-h exposures to 0.5- and 2.0-Torr hydrogen plasma at 350 °C.

series of etches as is illustrated in Fig. 2. The spectra were unchanged after the initial HF etch indicating that hydrogen in the oxide layer was not contributing to the observed signal. 1 μ of bulk silicon was then uniformly removed from both samples with Sirtl etch. A flat base line was observed for the single-crystal silicon sample. The spectrum of the etched polycrystalline sample was similar to that of the initial plasma-treated and etched samples, but the intensity of the peaks near 2100 cm^{-1} were substantially reduced. The 2019-cm^{-1} peak remained virtually unchanged and no evidence was found for the 2100-cm^{-1} peak in either poly- or single-crystal samples. An additional 2 μ were subsequently removed. Base-line noise increased appreciably in the polycrystalline sample due to increased surface roughness from the disparate rate of etch for various crystallites. The samples were then polished with 1/4-μ diamond paste and rerun, confirming that no 2100-cm^{-1} signal remained. The 2019-cm^{-1} peak again remained unchanged. The etch is sufficient to remove any weakly implanted hydrogen[16] or apparently any hydrogen incorporated in the thin damaged layer from polishing.

From zero-bias grain-boundary impedance measurements, it has previously been established[8] that the apparent grain-boundary hydrogen may be reversibly introduced and removed by successive plasma treatments and vacuum anneals (600 °C for 1 h), respectively. Figure 3 illustrates such a series of treatments on a polysilicon sample. The virgin vacuum annealed spectrum (A) shows no significant Si-H stretching modes in the region of interest. After hydrogenation for 12 h, a 2019-cm^{-1} peak is observed (B), which disappears upon vacuum anneal (C). (D) and (E) show, respectively, an identical treatment to (B) and then an extended 64-h treatment. The behavior of the 2019-cm^{-1} peak paralleled the established grain-boundary electrical measurements, suggesting that this peak is indeed associated with the hydrogen passivating the grain boundaries.

Applying the assignments of Brodsky[12] and Soule[11] from amorphous silicon to the peaks observed here indicates that peaks near 2000 cm^{-1} are characteristic of the SiH stretch due to SiH, and those above 2050 cm^{-1} are characteristic of SiH_2 or "surface" hydrogen. The 2019-cm^{-1} SiH peak is, therefore, assigned to the hydrogen stretching vibration of SiH. The surface hydrogen on the other hand may be bonded as SiH_2, although the surface nature of this species makes this assignment less certain.

After prolonged treatment in a hydrogen plasma, additional small but sharp absorption peaks are formed in polysilicon at 2007 and 1995 cm^{-1} as well as occasional small peaks between 2050 and 2100 cm^{-1} (e.g., 2083 and 2097 cm^{-1}). Etching shows that these peaks are not solely surface related, but they have different thermal desorption characteristics than the 2019 cm^{-1} peak. Temperatures greater than 600 °C are required to thermally desorb the species responsible for these peaks.

We cannot yet interpret all these peaks, but clearly FTIR is a powerful probe at the very small amounts of hydrogen incorporated during the plasma treatments. The peaks observed here are much sharper for the nonsurface Si-H bands

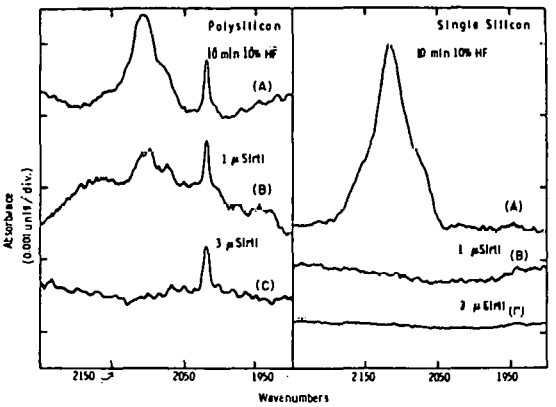

FIG. 2. FTIR spectra of single and polycrystalline silicon samples after (A) spectrum of samples in Fig. 1 after a subsequent 10-min etch in 10% HF. (B) 1 μm Sirtl etch. (C) Additional 2 μm Sirtl etch followed by polishing 1/4-μ diamond polish to remove surface roughness.

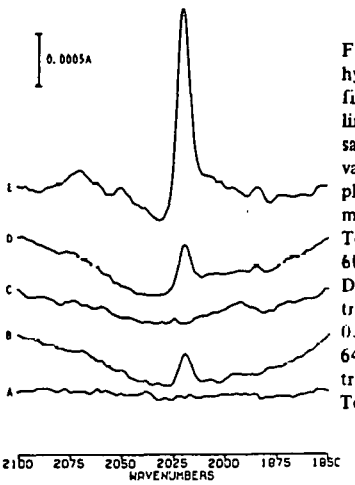

FIG. 3. FTIR spectra of hydrogen incorporated in fine-grained polycrystalline silicon. A. Fresh sample after 800 °C vacuum anneal. B. Sample after H-plasma treatment, 2 h, 400 °C, and 0.5 Torr. C. Sample after 1-h, 600 °C vacuum anneal. D. Sample after H-plasma treatment, 2 h, 400 °C, and 0.5 Torr. E. Sample after 64-h additional H-plasma treatment, 400 °C, and 0.5 Torr.

than those observed for amorphous silicon (FWHM is ~5 cm^{-1} vs > 50 cm^{-1} for amorphous silicon). The unique position and narrow linewidth at the 2019-cm^{-1} peak may enable it to serve as a marker for grain-boundary hydrogen in polycrystalline silicon.

Preliminary experiments on samples exposed to dc hydrogen plasma treatment show the presence of a strong 2019-cm^{-1} peak as well as very intense peaks at 2097 and 2083 cm^{-1}. These results will be presented later. Effects of surface treatment and dc and ac plasma parameters are currently being investigated. Methods are also being developed to quantify the amount of hydrogen incorporated into the silicon. Also, studies covering the spectral range between 5000 and 400 cm^{-1} are being initiated to utilize stretching, bending, and wagging Si-H and Si-D modes to better establish the structural nature of the incorporated hydrogen under different conditions.

We would like to thank R. Hellmer and F. T. Walder for technical assistance with these measurements and C. H. Seager for useful discussions of the data.

[1]For example, T. L. Chu, J. C. Lie, H. C. Mollenkopf, S. C. Chu, and K. W. Heizer, Sol. Energy 17, 229 (1975).
[2]C. H. Seager and T. A. Castner, J. Appl. Phys. 49, 3879 (1978).
[3]G. E. Pike and C. H. Seager, J. Appl. Phys. 50, 3414 (1979).
[4]C. H. Seager and G. E. Pike, Appl. Phys. Lett. 35, 709 (1979).
[5]C. H. Seager, G. E. Pike, and D. S. Ginley, Phys. Rev. Lett. 43, 532 (1979).
[6]D. R. Cambell, M. H. Brodsky, J. C. M. Hway, A. E. Robinson, and M. Albert, Bull. Am. Phys. Soc. 24, 435 (1979).
[7]C. H. Seager and D. S. Ginley, Bull. Am. Phys. Soc. 24, 401 (1979).
[8]C. H. Seager and D. S. Ginley, Appl. Phys. Lett. 34, 337 (1979).
[9]C. H. Seager and D. S. Ginley, Final Report-1979 SERI.
[10]C. H. Seager, D. S. Ginley, and J. D. Zook, Appl. Phys. Lett. 36, 831 (1980).
[11]D. E. Soule and A. T. Reedy, Thin Solid Films 63, 175 (1979).
[12]M. H. Brodsky, M. Cardona, and J. J. Cuomo, Phys. Rev. B 16, 3556 (1977).
[13]J. C. Knights, A. Lucousky, and R. J. Nemanich, Philos. Mag. B 37, 467 (1978).
[14]E. C. Freeman and W. Paul, Phys. Rev. B 18, 4288 (1978).
[15]A. E. Becker and G. W. Gobeli, J. Chem. Phys. 38, 2942 (1963).
[16]H. J. Stein and P. S. Peercy, Phys. Rev. B 22, 6233 (1980).
[17]P. R. Griffiths, *Chemical Infrared Fourier Transform Spectroscopy* (Wiley, New York, 1975).

APPENDIX C

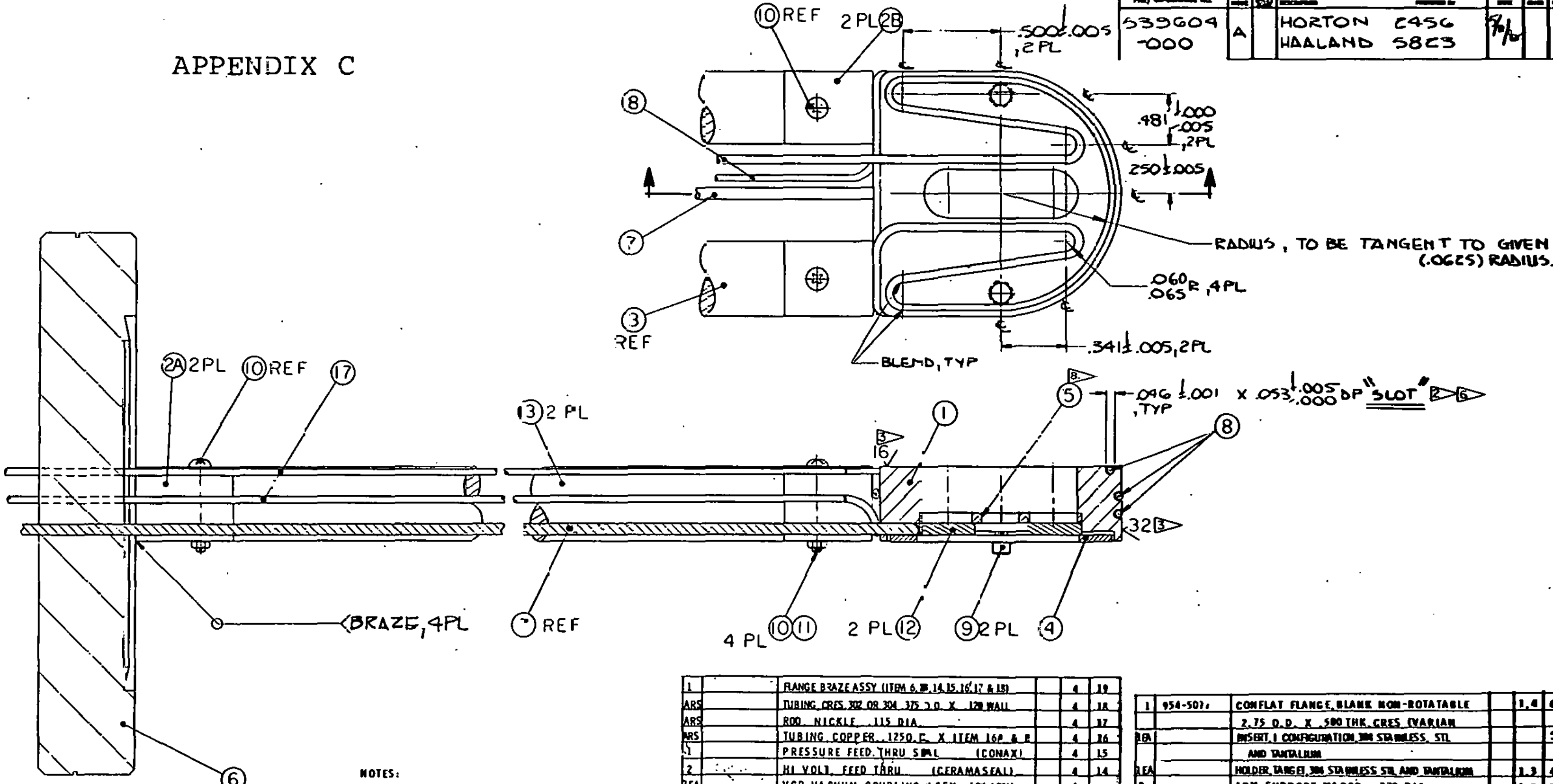

539604 -000	A	HORTON 2456	HAALAND 5823

NOTES:

1. GENERAL REQUIREMENTS PER #900010.
2. ITEM 1 TO BE MACHINED IN TWO PHASES. PHASE ONE PRIOR TO BRAZING OF HEATING ELEMENTS. (USE NO SULFUR BEARING LUBRICATES).
3. ITEM 1 TO BE MACHINED IN TWO PHASES. PHASE TWO AFTER BRAZING OF HEATING ELEMENTS. (USE NO SULFUR BEARING LUBRICATES).
4. RADIUS AS SHOWN.
5. BOTTOM OF (.062) Ø THRU HOLE TO BE TANGENT TO SURFACE "E" WITHIN ±.003 AFTER "I" CONFIGURATION INSERT (ITEM 12) IS IN PLACE.
6. (.046) WIDE SLOTS ON SURFACE "F" (ITEM 1) ARE DEFINED ON SHT 1.
7. ITEM 2A & 2B DIFFER, IN THER (.375) DIA. LENGTHS AND ITEM 2B'S RADIUSED SHOULDER (USE NO SULFUR BEARING LUBRICATES.
8. ITEM 12 IS TO BE MADE OUT OF 304 CRES AND TANTALIUM.
9. REMOVE ALL SHARP CORNERS.

1		FLANGE BRAZE ASSY (ITEM 6, 13, 14, 15, 16, 17 & 18)		4	19
ARS		TUBING, CRES, 302 OR 304 .375 O.D. X .120 WALL		4	18
ARS		ROD, NICKLE, .115 DIA.		4	17
ARS		TUBING, COPPER, .1250.E. X ITEM 16A & B		4	16
1		PRESSURE FEED. THRU SEAL (CONAX)		4	15
2		HI VOLT. FEED THRU (CERAMASEAL)		4	14
2EA		VCR VACUUM COUPLING ASSY (CAJON)		4	
2	SS-2-VCR-1	VCR FEMALE NUT, 5/16-24UNF-2B			
2	SS-2-VCR-4	VCR MALE NUT, 5/16-24UNF-2A			
4	SS-2-VCR-3	VCR GLAND 1/8 TUBE SOCKET			
5	SS-2-FCR-2	VCR GASKET 1/8 I.D.			
2		TARGET, SILICON		1	12
4		NUT, PLAIN, CRES #2-56UNC-2B		1	11
4	NAS1635	SCREW, MACH, PAN-HD., CRES #2-56UNC-2A		1	10
		X .50 LONG SHANK			
2	MS16995-11	SCREW, SOC HD-HEX, STAINLESS STL		1	9
		4-40UNC-3A X .500 LNG			
ARS		HEATING ELEMENT, THERMOCOAX, .0393 STOCK DIA.		1	8
		(AMPEREX ELECTRONIC CORP)			
1		THERMOCOUPLE TYPE K (OMEGA OR EQUIVALENT)		1	7
		CRES SHEATH			

1	954-5071	CONFLAT FLANGE, BLANK NON-ROTATABLE		1,4	6
		2.75 O.D. X .500 THK. CRES (VARIAN			
1EA		INSERT, I CONFIGURATION, 304 STAINLESS, STL			5
		AND TANTALIUM			
1EA		HOLDER, TARGET, 304 STAINLESS STL AND TANTALIUM		1,3	4
2		ARM, SUPPORT, MACOR, .375 DIA.		1,3	3
2		CONNECTOR, BODY TO ARM, CRES 304, .375 DIA.		1,3	2B
2		CONNECTOR, FLANGE TO ARM, CRES 304, .375 DIA.		1,3	2A
1		BODY, TARGET, 304 STAINLESS STL, .375 THK	2,3	1,2	1

LIST OF MATERIAL

SHEET 1 2 3 4

UNCLASSIFIED

UNCLASSIFIED

SILICON SAMPLE HOLDER TARGET ASSY

D 14213 539604

SCALE 4/1 SHEET 1 OF 4

539604

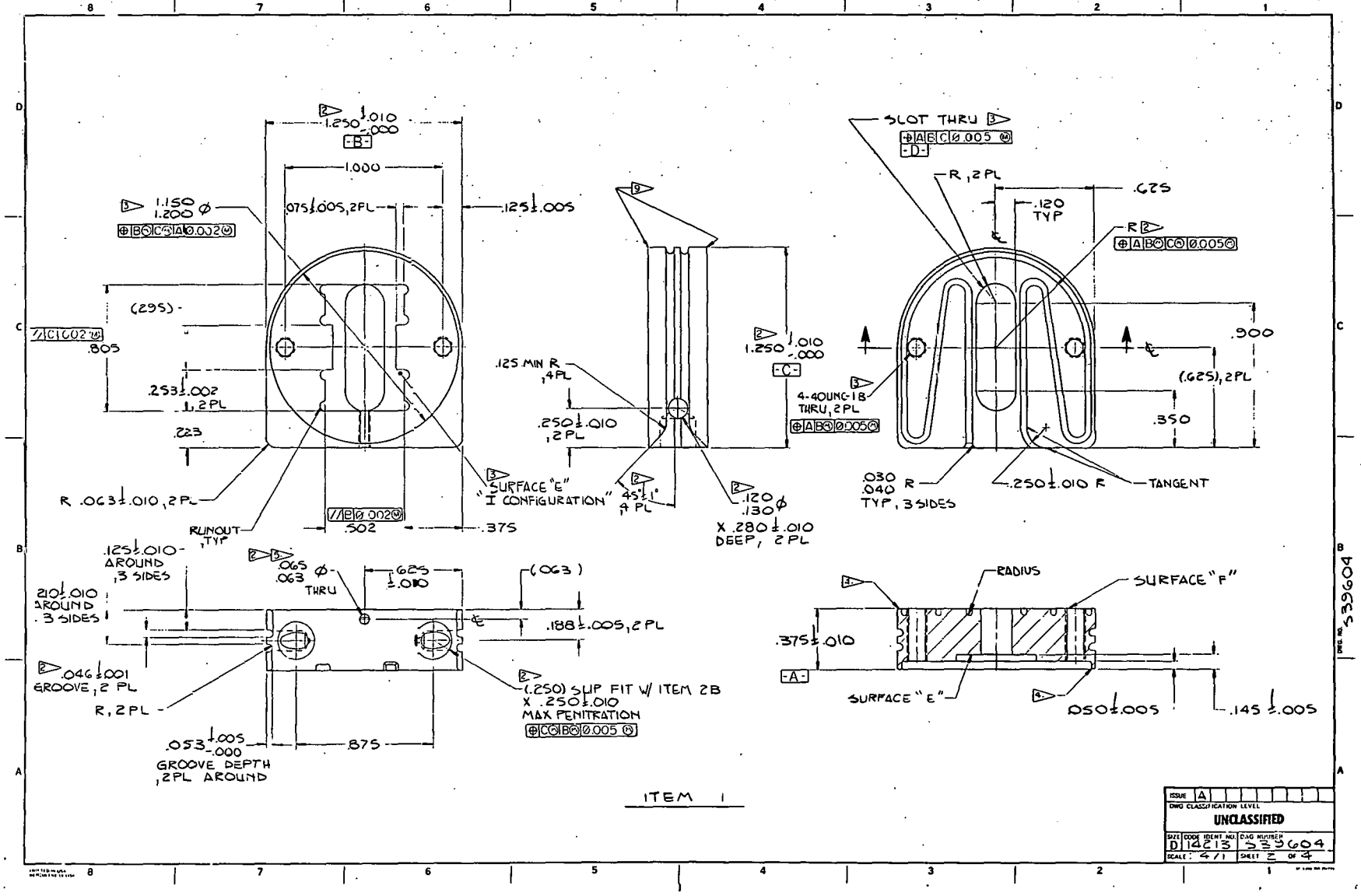
1.250 +.010 -.000
-B-
1.000
1.150 Ø
1.200
.075±.005, 2PL
.125±.005
(.295)
.805
.253±.002
1, 2PL
.223
R .063±.010, 2PL
RUNOUT TYP
.502
.375
SURFACE "E"
"I CONFIGURATION"
.125 MIN R
, 4PL
.250±.010
, 2PL
45°±1°
4 PL
.120
.130 Ø
X .280±.010
DEEP, 2 PL
1.250 +.010 -.000
-C-
SLOT THRU
-D-
R, 2PL
.625
.120
TYP
R
.900
(.625), 2PL
.350
4-40UNC-1B
THRU, 2PL
.030
.040
TYP, 3 SIDES
.250±.010 R
TANGENT
.125±.010
AROUND
, 3 SIDES
.210±.010
AROUND
, 3 SIDES
.065 Ø
.063
THRU
.625
±.010
(.063)
.188±.005, 2PL
.046±.001
GROOVE, 2 PL
R, 2PL
.053 +.005 -.000
GROOVE DEPTH
, 2PL AROUND
.875
(.250) SLIP FIT W/ ITEM 2B
X .250±.010
MAX PENITRATION
RADIUS
SURFACE "F"
.375±.010
-A-
SURFACE "E"
.050±.005
.145±.005
ITEM 1
ISSUE A
DWG CLASSIFICATION LEVEL
UNCLASSIFIED
SIZE D
CODE IDENT. NO. 14213
DWG NUMBER 339604
SCALE 4/1
SHEET 2 OF 4
DWG NO. 339604

NOTES:

1. FOR GENERAL REQUIREMENTS SEE 9900000.
2. DEWAR SEAL CONTOUR TO BE AS SHOWN, SO THAT SURFACE CAN BE GROUND FLUSH AROUND AT BOTH ENDS TO ACCEPT ITEM 5'S ADHERING AT ASSY.

DESIGN AGENCY PART OR CONTROL NO.	REVISIONS					
	LTR	STATUS	DESCRIPTION	APPROVED BY	DATE	
539253 -000	A		HORTON 2456 HAALAND 5825		5/11/72	

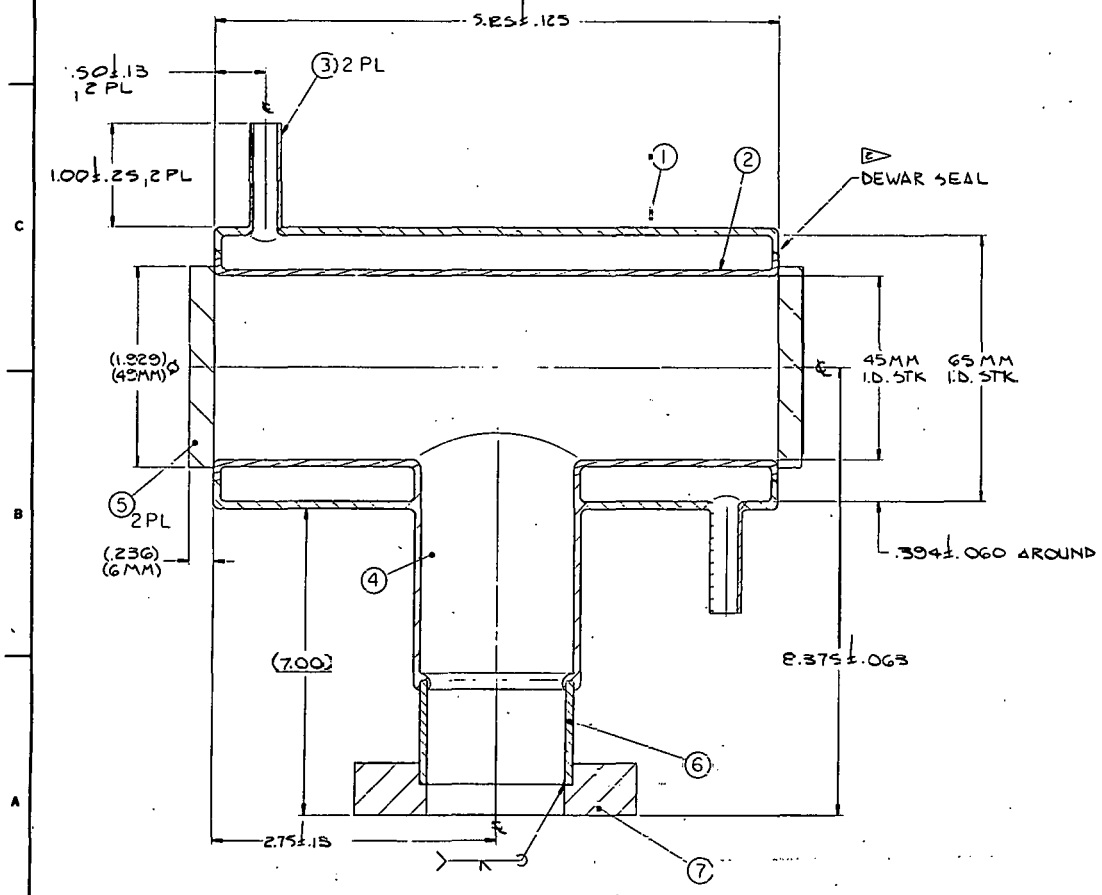

SECTION VIEW

1		CONFLAT, FLANGE, 1 1/2" I.C. NON-ROTATABLE X 2.75" O.D., CRES, (VARIAN ASSOC.)		7
1	5S285447	TUBING, KOVAR, 1.50" O.D. X 1.48" I.D.		6
2		WINDOW, STANDARD INFRARED, K Br, 49 MM DIA. X 6 MM THK (HARSHAW CO.)		5
ARS		GRADED QUARTZ TO KOVAR SEAL 38 MM + 1 MM I.D. X 1.5 MM + .5 MM WALL		4
ARS		TUBING, QUARTZ, CLEAR FUSED, 6 MM I.D. X 1 MM WALL THK'NESS		3
ARS		TUBING, QUARTZ, CLEAR FUSED, 45 MM I.D. X 1.5 MM WALL THK'NESS		2
ARS		TUBING, QUARTZ, CLEAR FUSED, 65 MM I.D. X 2 MM WALL THK'NESS		1
NA	9900000	GENERAL REQUIREMENTS		

LIST OF MATERIAL

AGENCY APPROVALS			SHEET	1	TITLE
ORG	DATE	APPROVALS	ISSUE	A	WATER JACKETED QUARTZ VACUUM FIXTURE ASSY
			SHEET INDEX		
PART CLASSIFICATION: UNCLASSIFIED					
DWG CLASSIFICATION LEVEL: UNCLASSIFIED			SIZE: D	CODE IDENT. NO.: 14215	DWG NUMBER: 539253
			SCALE: 2/1	SHEET 1 OF 1	

539253 DWG NO.

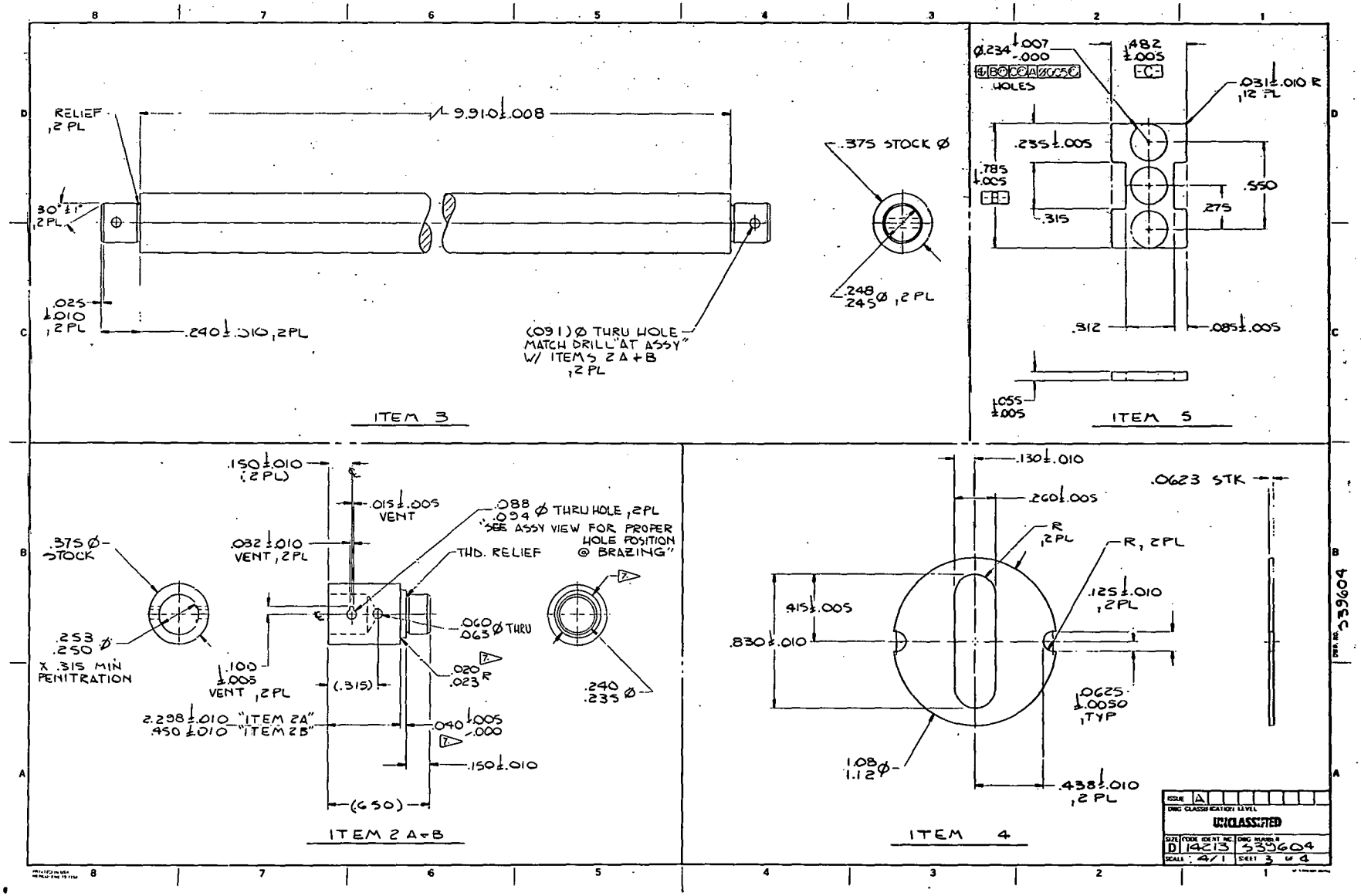
RELIEF ,2 PL
9.910±.008
30°±1° ,2 PL
.025 ±.010 ,2 PL
.240±.010 ,2 PL
(.091)Ø THRU HOLE MATCH DRILL AT ASSY W/ ITEMS 2A+B ,2 PL
.375 STOCK Ø
.248 .245 Ø ,2 PL
ITEM 3
Ø.234 +.007 -.000 .HOLES
.482 ±.005
-C-
.031±.010 R ,12 PL
.235±.005
.785 ±.005
.550
.275
.315
.312
.085±.005
.055 ±.005
ITEM 5
.150±.010 (2 PL)
.015±.005 VENT
.088 .094 Ø THRU HOLE ,2PL "SEE ASSY VIEW FOR PROPER HOLE POSITION @ BRAZING"
.375 Ø STOCK
.032±.010 VENT ,2 PL
THD. RELIEF
.253 .250 Ø
X .315 MIN PENITRATION
.060 .063 Ø THRU
.020 .023 R
.100 ±.005 VENT ,2 PL
(.315)
2.298±.010 "ITEM 2A"
.490±.010 "ITEM 2B"
.040 +.005 -.000
.150±.010
(.650)
.240 .235 Ø
ITEM 2A+B
.130±.010
.0623 STK
.260±.005
R ,2PL
R, 2PL
.125±.010 ,2PL
.415±.005
.830±.010
.0625 ±.0050 ,TYP
1.08 1.12 Ø
.438±.010 ,2 PL
ITEM 4
ISSUE A
DRG CLASSIFICATION LEVEL
UNCLASSIFIED
SIZE D
CODE IDENT NO. 14213
DRG NUMBER 539604
SCALE 4/1
SHEET 3 of 4

539604

1A ITEM 14 (2PL) TO BE BRAZED INTO ITEM 6'S (.3625 D) C'BORE, AS SHOWN, AT ASSY.

2A ITEM 13 (2PL) TO BE BRAZED TO ITEM'S 16 A&B AT ASSY.

3A ITEM 28 (2PL) TO BE BRAZED, AS SHOWN, AT ASSY.

4A ITEM 19 TO BE 3.00 ± .02 LONG W/A .205 DIA +.210 −.215 X .210 ± .005 DEEP C'BORE, ONE END, AS SHOWN. BRAZE ITEM 19 TO ITEM 6 FLUSH, AS SHOWN, AT ASSY.

5A ITEM 15'S 1/8-27 NPT MALE THREAD IS TO BE REMOVED AND TURNED DOWN TO A 4.2075 D SLIP FIT W/ ITEM 19, WHEN BRAZED INTO PLACE, AS SHOWN, AT ASSY.

NOTE: CONT.

6A ITEM 17 (2PL) OVERALL LENGTH TO BE 17.00 ± .13 X .115 DIA W/ .031 DIA HOLE ± .015 DRILLED .256 ± .010 DP, BOTH ENDS. ITEM 17 IS TO BE BRAZED AT TOP OF ITEM 14 @ ASSY.

7A ITEM "16A" IS TO BE 4.00 ± .02 LONG AND IS TO BE BRAZED TO ITEM 16 @ 13, AS SHOWN, AT ASSY.
ITEM "16 B" IS TO BE 16.00 ± .02 LONG AND IS TO BE BRAZED TO ITEM 16 @ 13, AS SHOWN, AT ASSY.

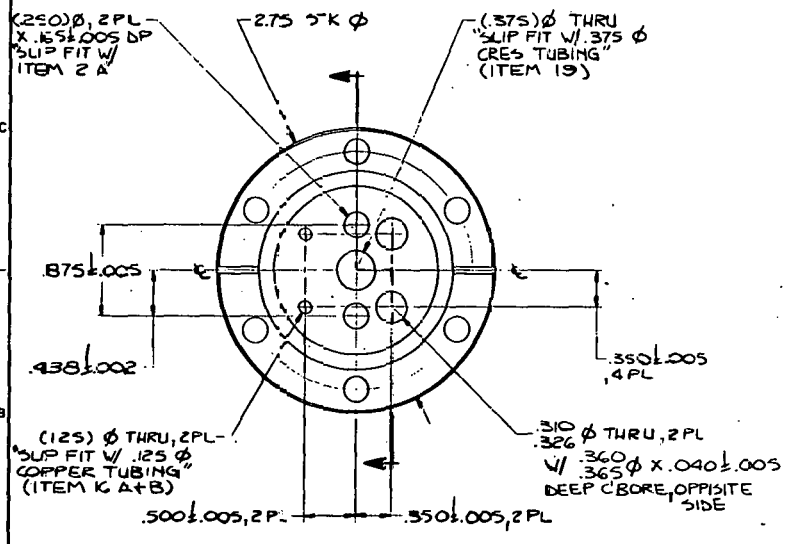

NOTE:
TOP VIEW SHOWS ITEM 6 ONLY.

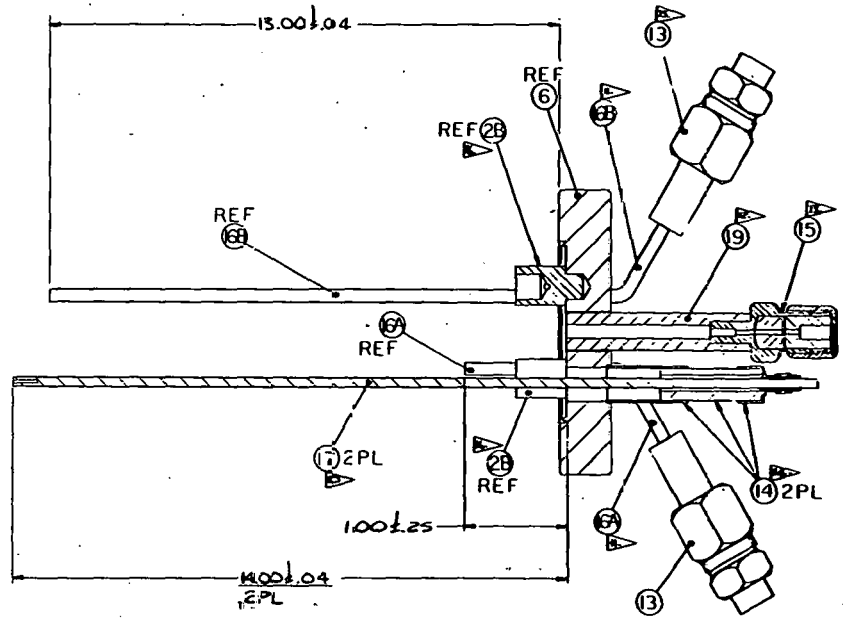

ITEM 19

		A
	D4213	535604
	SCALE: 2/1	SHEET 4 OF 4

APPENDIX D

Modification of grain boundaries in polycrystalline silicon with fluorine and oxygen

David S. Ginley

Sandia National Laboratories[a] Organization 5154 Albuquerque, New Mexico 87185

(Received 11 May 1981; accepted for publication 4 August 1981)

Hydrogen plasmas have been shown to significantly reduce barrier heights and recombination center densities in the grain boundaries in polycrystalline silicon. These results have stimulated interest in the use of other modifying agents. We demonstrate here that the exposure of *n*-type polycrystalline silicon to fluorine and oxygen in molecular and atomic forms can result in increased potential barrier heights. This has implications for the development of silicon varistors and capacitors for use in integrated circuits.

PACS numbers: 81.40.Rs, 72.40. + w, 85.20.Ea, 78.50.Ge

The chemical modification of grain boundaries has attracted considerable interest as a means of improving the performance of polycrystalline silicon photovoltaic cells.[1-3] Our previous successful work on the hydrogen passivation of polycrystalline silicon grain boundaries led us to investigate a number of other chemical reagents as possible passivating agents.

We report here for the first time that grain boundary potential barriers in polycrystalline silicon can be significantly increased by exposure to F_2 and O_2 in both molecular and atomic forms.

Varistors are seeing increased usage as current surge protectors.[4-6] Silicon based devices would be quite attractive. Their usage would require the largest possible barrier heights. There is also appreciable interest in developing Si based capacitors for bulk and integrated circuit applications.

[a]A. U.S. Department of Energy Facility.

 0003-6951/81/200624-03$00.50

The ability to selectively increased potential barriers is of great potential use in both of these areas.

The silicon samples employed in this study were obtained from a number of different sources. *n*-type materials used were 2-Ω cm melt-doped Monsanto float zone refined, large grained polysilicon (grain size 0.1–1 mm), Texas Instruments CVD fine grained (25–100-μm grain size), neutron transmution doped polysilicon with a doping level of approximately 2×10^{14} P/cm^3, and single-crystal Monsanto silicon, neutron transmutation doped to 8×10^{14} P/cm^3. *p*-type materials employed were Honeywell polysilicon produced by the dip-coating silicon on ceramic process and melt doped to $\sim2\times10^{16}$ B/cm^3, and Wacker cast polysilicon with a doping level of 10^{15} B/cm^3 or below.

The dc plasma apparatus employed has been described previously.[7] When fluorine was employed, the gases were routed through graphite then KOH traps previous to the pump. Typical conditions were ~5 Torr (F_2 20% in He), 640°C, and 10-mA total plasma current at 500–800 Vdc for 1 h and for oxygen 5 Torr O_2, 640°C, 10-mA total plasma current, 500–600 Vdc. Experiments without plasmas were performed similarly.

Vacuum anneals were performed in a similar turbomolecular pumped apparatus to a base system pressure of 1×10^{-7} Torr.

Conductivity changes were measured with the drag trace apparatus discussed previously.[8,9] Activation energies were determined by monitoring conductance as a function of temperature using a thermoelectric heater-cooler on the stage of the drag trace apparatus.

Outgassing experiments were conducted in an ion pumped vacuum chamber (base pressure 2×10^{-9} Torr) equipped with a micro-platinum tube furnace with a quartz liner. The ionizer of a UTI 100 C quadrapole mass spectrometer was mounted directly above the sample. The furnace was driven by a programmed constant current supply.

The nature of the virgin state is always somewhat difficult to adequately define when looking at grain boundary properties, since they are very sensitive to previous surface treatments and anneals. We have found that etching all samples roughly 25 μ with Sirtl etch ($CrO_3/HF/H_2O$) removes most of surface damage layer from cutting and polishing. This was done for all samples except the Honeywell which (as a consequence of the dip process) does not have a heavily damaged surface region. All samples were then annealed at 600 or 800 °C in vacuum before any other treatments. These treatments in effect define our virgin state. The 600 °C anneal had virtually no effect on barrier impedances while the 800 °C anneal often resulted in increases in barrier heights. This may be associated with the diffusion of residual oxgen in the vacuum system into the grain boundaries.

The exposure of large grained, melt-doped, Monsanto *n*-type polysilicon to plasmas of F_2 or O_2 resulted in substantial increases in the average barrier height as determined by drag trace measurements. Treatments with no plasma result in similar but less spectacular changes. CF_4 plasmas were nearly as effective as those with F_2 but carbon deposition was somewhat of a problem. For 1-h plasma treatments at 650 °C, 10-mA plasma current and a positive sample bias, typical results for F_2 treatments are initial average resistivity/boundary (seven boundaries) 520 Ω; final 12 350 Ω. The maximum resistance increases per boundary observed have been factors on the order of 250 times. For similar conditions, typical results for O_2 plasma treatments are initial average resistivity/boundary (six boundaries) 57.6 Ω; final 344 Ω. The maximum changes per boundary for O_2 plasmas have been factors of around 20. We have previously found that for hydrogen passivation experiments, the presence of *atomic* hydrogen was necessary to see significant changes in boundary conductance.[1] That molecular species are effective in the case of F_2 and O_2 probably reflects the fact that they both interact strongly and exothermically with the silicon surface.[10,11] Samples vacuum annealed at 800 °C and then treated in F_2 plasmas at 640 °C showed increases in boundary impedance at both the anneal step and upon plasma treatment. Subsequent 800 °C vacuum anneal returned impedance to at or below the levels of the first 800 °C anneal. In general, direct plasma fluorination is more effective than vacuum anneals at 800 °C followed by F_2 plasma treatments.

Plasma treatments with fluorine show increases in barrier impedance at temperatures as low as 400 °C. The process is optimized at 650 °C.

Monitoring sample conductance as a function of thickness during etching experiments yields information on penetration depth for various treatments.[12] Etching experiments on plasma fluorinated samples show penetration of the fluorine throughout the sample. Because of the large changes in boundary resistance observed it is unlikely that any region of substantially lower impedance remains in the sample.

Table I illustrates activation energy changes for some boundaries in Monsanto material before and after plasma fluorination. Arrhenius plots were obtained for conductance versus inverse temperature. The changes are more pronounced for originally small barriers than for large ones. Some of the barriers are increased to near the maximum value of 0.62 eV observed previously for *n*-type silicon.[13] The fact that we have seen no barriers greater than 0.62 eV is interesting and may indicate that only states above the neutral Fermi level[14] can be introduced or changed with fluorine. These states seem to be related to the same ones that interact with hydrogen plasmas. We have observed that plasma hydrogenations are much more difficult after fluorination. Previously flourinated samples showed hydrogen penetra-

TABLE I. Impedance and activation energy data for the fluorination of n-type polycrystalline silicon.

Sample	Conditions	Individual Boundaries (Impedance--Activation Energy)	
20OM7 17	VIRGIN [a]	162Ω--0.23eV	974Ω--0.50eV
	F2 PLASMA	10 746Ω--0.54eV	10 087Ω--0.62eV
20CM7-2	VIRGIN [b]	250Ω--0.28eV	169Ω--0.34eV
	F2 PLASMA [c]	6 136Ω--0.56eV	1 591Ω--0.45eV

[a] 650 °C anneal vacuum 1 hour.
[b] 800 °C anneal vacuum 1 hour.
[c] Same conditions as 7-17 1 hour 665 °C 20 torr F2/He.

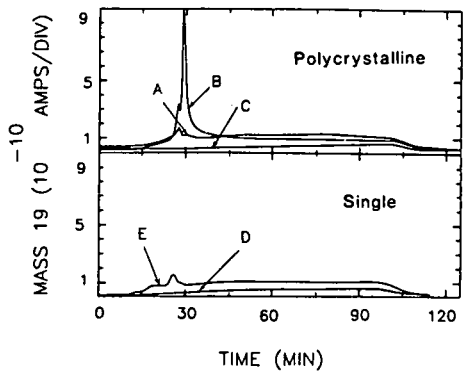

FIG. 1. Outgassing experiments where mass 19 intensity plotted as electron multiplier current is monitored as a function of time. Temperature vs time profiles were identical for all runs and consist of a programmed increase to 610°C in 50 min and a maintenance of this temperature for another hour. In the upper portion of the figure, A is an annealed polysilicon sample, B is annealed and then fluorine treated polycrystalline silicon sample, and C is the same sample as B outgassed again *in situ*. In the lower portion of the figure, D is an annealed single-crystal silicon sample and E is an annealed and fluorine treated single-crystal silicon sample.

tion to one-third the depth of identical samples not previously exposed to fluorine. Linear Arrhenius plots were obtained for fine grained Texas Instruments' n-type polycrystalline silicon before (850 °C vacuum anneal) and after plasma fluorination (1 h, 643 °C, 10 mA, 650 V). Data were obtained by monitoring the current necessary to maintain a constant voltage drop across the sample as a function of temperature from + 5 to + 90 °C. The average activaton energy for the whole sample went from 0.116 eV in the annealed state to 0.460 eV after fluorination. These experiments clearly show that the density of states and the size of the double depletion regions are increasing upon fluorination. The same is probably true for oxygen since qualitatively similar results are obtained for plasma oxygenation.

A series of mass spectrometric outgassing experiments were conducted to try and directly observe any fluorine in the boundaries. Fine grained Texas Instruments polycrystalline silicon samples and Monsanto single-crystal silicon samples ($2\times5\times10$ mm) were plasma fluorinated for 1 h at 10 mA and 640 °C after an 800 °C vacuum anneal. Control samples were just annealed at 800 °C in vacuum. Samples were etched approximately 110 μm with Sirtl and then outgassed separately in the mass spectrometer. Representative data are illustrated in Fig. 1. Some background is always observed as a consequence of surface fluorine from the etch. Both the single and the polycrystalline samples show significant fluorine outgassing. The peak at 27 min (350 °C) is apparently associated with bulk fluorine. A peak at 30 min (420 °C) occurs only in the polycrystalline samples and is most probably associated with fluorine in the grain boundaries. As curve C on the top of Fig. 1 illustrates, a second outgassing cycle releases no additional fluorine. In the outgassing experiments all of the fluorine of interest is removed from the samples by 500 °C while samples that were not etched show a return to virgin electrical properties only between 650 to 800 °C. To determine whether this effect was due to a surface layer or an intrinsic difference in the states being examined, a series of samples were outgassed at 400 °C after being etched to different depths and the conductance monitored. It was found that samples etched from 1 to 5 μ showed a return to the prefluorinated state after aneals of 1 h at 400 °C. Thus a thin layer forms upon fluorination that subsequently impedes fluorine diffusion. The effect is not as pronounced for samples treated in molecular fluorine.

Fluorine treatments of p-type Honeywell or Wacker material showed little changes in boundary impedances. In typical experiments where the boundary resistivity in n-type material changed an average of 150× Honeywell material showed increases of an average of 1.04×.

The lack of interaction with p-type material may indicate that the (electron) states the fluorine affects are already empty in this case and thus the amount of trapped holes in the boundary does not increase.

In summary, fluorine and oxygen treatments of n-type polysilicon increase barrier heights and density of states for the grain boundaries. A maximum activation energy greater than the highest for virgin silicon (0.62 eV) has not been observed though factors of greater than 250 times have been observed for conductivity changes of some barriers. p-type material seems relatively unaffected by exposure to fluorine. The mass spectrometric experiments indicate as well that fluorine is quite mobile at relatively low temperatures in both single and polycrystalline silicon. An optimization of the fluorination process is underway along with an investigation to directly identify the states involved.

This work was supported by the U.S. Department of Energy under Contract DE-AC04-76-DP00789. The technical assistance of R. P. Hellmer in treating the samples and making the electrical measurements is gratefully acknowledged, as are many helpful discussions with C. H. Seager.

[1]C. H. Seager and D. S. Ginley, Appl. Phys. Lett. **34**, 337 (1979).
[2]D. R. Campbell, M. H. Brodsky, J. C. M. Hway, A. E. Robinson, and M. Albert, Bull. Am. Phys. Soc. **24**, 435 (1979).
[3]C. H. Seager, D. S. Ginley, and J. D. Zook, Appl. Phys. Lett. **36**, 831 (1980).
[4]J. D. Harnder, F. O. Martzoff, W. G. Morris, and F. D. Golder, Electronics **45**, 91 (1972).
[5]Structural properties of: D. R. Clarke, J. Appl. Phys. **49**, 2407 (1978).
[6]Electrical properties of: G. D. Mahan, L. M. Levinson, and H. R. Philip, J. Appl. Phys. **50**, 2799 (1979).
[7]C. H. Seager and D. S. Ginley, "Fundamental Studies of Grain Boundary Passivation in Polycrystalline Silicon with Application to Improved Photovoltaic Devices", Research Report Covering January to July 1980, SAND80-2461, pp. 40.
[8]D. S. Ginley, M. A. Butler, and C. H Seager, *Solar Materials Science* (Academic, New York, 1980), Chap. 18, p. 619.
[9]C. H. Seager and T. G. Castner, J. Appl. Phys. **49**, 3879 (1978).
[10]R. Landau, Corrosion **8**, 283 (1952).
[11]C. E. Wicks and F. E. Block, Bureau of Mines Bulletin 605, U. S. Gov. Printing Office, Washington 1963.
[12]C. H. Seager and D. S. Ginley, J. Appl. Phys. **52**, 1050 (1981).
[13]G. E. Pike and C. H. Seager, Adv. Ceramics **1**, 53 (1981).
[14]The neutral Fermi level is the Gibbs free energy (electro-negativity) for the electron in the neutral grain boundary region before charge flows from the grains. Observationally it appears to be the same for all of the polycrystalline silicon examined thus far. The observed position near midgap results in a maximum barrier height of ~0.62 eV.

Unlimited Distribution

Distribution:

Amex Systems, Inc.
Attn: M. R. Caldera
3355 El Segundo Blvd.
Hawthorne, CA 90250

Brown University
Division of Engineering
Attn: John Shewchun
Providence, RI 02912

Case Western Reserve University
Attn: Prof. A. H. Heuer
Metallurgy Department
Cleveland, OH 44106

Colorado State University
Electrical Engineering Dept.
Attn: Prof. J. DuBow
Fort Collins, CO 80523

Columbia University
Department of Elect. Eng.
and Computer Science
Attn: Prof. E. S. Yang
1312 Mudd Building
New York, NY 10027

Crystal Systems, Inc.
Attn: C. P. Khattak
Shetland Industrial Park
35 Congress Street
Salem, MA 01970

EIC Corporation
Attn: Dr. R. D. Rauh
55 Chapel Street
Newton, MA 02158

Energy Materials Corp.
Attn: David N. Jewett
Ayer Road
Harvard, MA 01451

Exxon Research and Eng. Co
Attn: Dr. A. K. Ghosh
Exxon Research Center
Building 1-3006
Linden, NJ 07036

Honeywell Technical Center
Attn: J. D. Heaps
10701 Lyndale Ave. South
Bloomington, MN 55420

The Johns Hopkins University
Applied Physics Laboratory
Attn: Dr. C. Feldman
Johns Hopkins Road
Laurel, MD 20810

Jet Propulsion Laboratory
Attn: Dr. Kris Koliwad
4800 Oak Grove Drive
Pasadena, CA 91103

Motorola, Inc.
Solar Energy Department
Attn: Dr. I. A. Lesk
5005 East McDowell Road
Phoenix, AZ 85008

Oak Ridge National Laboratory
Solid State Division
Attn: Richard F. Wood
P. O. Box X
Oak Ridge, TN 37830

Pennsylvania State Univ.
Attn: Stephen J. Fonash
Engineering Sciences Program
127 Hammond Bldg.
University Park, PA 16802

Phrasor Scientific, Inc.
Attn: Julius Perel
1536 Highland Avenue
Duarte, CA 91010

Poly Solar, Inc.
Attn: Dr. T. L. Chu
2701 National Drive
Garland, TX 75041

RCA Laboratories (3)
Attn: Dr. B. W. Faughnan
D. Redfield
R. D'Aiello
P. O. Box 432
Princeton, NJ 08540

Distribution (continued):

University of Florida
Dept. of Electrical Engin.
Attn: Prof. F. A. Lindholm
Gainesville, FL 32611

Rockwell International Corp.
Electronics Research Center
Attn: Dr. R. P. Ruth
3370 Miraloma Avenue
Anaheim, CA 92803

J. C. Schumacher Co.
Attn: E. B. Moore
580 Airport Road
Oceanside, CA 92054

Sensor Technology
Attn: Sanjeev Chitre
21012 Lassen Street
Chatsworth, CA 91311

Siltec Corporation
Attn: Anthony Bonora
3717 Haven Avenue
Menlo Park, CA 94025

Solarex Corporation (2)
Attn: G. Storti
W. Regnault
1335 Piccard Drive
Rockville, MD 20850

SRI International
Attn: Dr. S. R. Morrison
333 Ravenswood Avenue
Menlo Park, CA 94025

State University of New York
at Buffalo
Dept. of Electrical Engin.
Attn: Prof. W. A. Anderson
4232 Ridge Lea Road
Amherst, NY 14226

Westinghouse R&D Center
Attn: Dr. J. R. Szedon
1310 Beulah Road
Pittsburgh, PA 15235

Westinghouse R&D Center
Attn: Dr. W. R. Gass
1310 Beulah Road
Pittsburgh, PA 15235

8266	E. A. Aas
3141	L. J. Erickson (5)
3151	W. L. Garner (3)
3154-3	C. H. Dalin for DOE/TIC (25)
1000	J. K. Galt
1100	F. L. Vook
1130	G. A. Samara
1132	C. H. Seager (50)
1150	J. E. Schirber
1154	D. S. Ginley

Org.	Bldg.	Name	Rec'd by	Org.	Bldg.	Name	Rec'd by

Sandia National Laboratories